bioRxiv preprint doi: https://doi.org/10.1101/481457; this version posted December 26, 2018. The copyright holder for this preprint (which was not certified by peer review) is the author/funder. All rights reserved. No reuse allowed without permission.

CBP/EP300-dependent acetylation and stabilization of HSF2 are compromised in the rare disorder, Rubinstein-Taybi syndrome

Aurélie de THONEL[1,2,3,§,&], Johanna K. AHLSKOG[4,5,§], Ryma ABANE[1,2,3], Geoffrey PIRES[1,2,3], Véronique DUBREUIL[1,2,3], Jérémy BERTHELET[2,6], Anna L. AALTO[4,5], Sarah NACERI[1,2,3], Marion CORDONNIER[8,9,10], Carène BENASOLO[1,2,3], Matthieu SANIAL[2,11], Agathe DUCHATEAU[1,2,3], Anniina VIHERVAARA[4,5,Ψ], Mikael C. PUUSTINEN[4,5], Federico MIOZZO[1,2,3,θ], Mathilde HENRY[1,2,3,ξ,£], Déborah BOUVIER[1,2,3], Jean-Paul CONCORDET[12,13,14], Patricia FERGELOT[15,16], Élise LEBIGOT[17], Alain VERLOES[3,18,19,20,21], Pierre GRESSENS[2,3,18,22], Didier LACOMBE[15,16], Jessica GOBBO[8,9,10], Carmen GARRIDO[8,9], Sandy D. WESTERHEIDE[23], Michel PETITJEAN[2,7], Olivier TABOUREAU[2,7], Fernando RODRIGUES-LIMA[2,6], Madeline LANCASTER[24], Sandrine PASSEMART[3,18,19,20,21], Délara SABÉRAN-DJONEIDI[1,2,3], Lea SISTONEN[4,5,&,*], Valérie MEZGER[1,2,3,&,*]

[1]CNRS, UMR7216 Épigénétique et Destin Cellulaire, F-75205 Paris Cedex 13, France,
[2]Univ Paris Diderot, Sorbonne Paris Cité, F-75205 Paris Cedex 13, France,
[3]Département Hospitalo-Universitaire DHU PROTECT, Paris, France.

[4]Faculty of Science and Engineering, Åbo Akademi University, Turku, Finland,
[5]Turku Centre for Biotechnology, University of Turku and Åbo Akademi University, Turku, Finland.

[6]Unité BFA, CNRS UMR 8251 Biologie Fonctionnelle et Adaptative (BFA), F-75205 Paris Cedex 13, France.

[7]Inserm UMR-S 973 Molécules Thérapeutiques in silico (MTi), F-75205 Paris Cedex 13, France

[8]INSERM, UMR1231, Laboratoire d'Excellence LipSTIC, Dijon, France.
[9]University of Bourgogne Franche-Comté, Dijon, France.
[10]Département d'Oncologie médicale, Centre Georges-François Leclerc, Dijon, France.

[11]CNRS, UMR 7592 Institut Jacques Monod, Paris F-75205, France.

[12]Muséum National d'Histoire Naturelle, 75231 Paris Cedex 05, France.
[13]CNRS UMR 7196, 75231 Paris Cedex 05, France.
[14]INSERM U1154, 75231 Paris Cedex 05, France.

[15]Laboratoire Maladies Rares: Génétique et Métabolisme (MRGM), Université de Bordeaux, INSERM U1211, Bordeaux, France.
[16]Department of Medical Genetics, CHU de Bordeaux, Bordeaux, France.

[17]Service de biochimie-pharmaco-toxicologie, Hôpital Bicêtre, Hopitaux Universitaires Paris-Sud, 94270 Le Kremlin Bicêtre, France

[18] UMR 1141 PROTECT, INSERM, Université Paris Diderot, Sorbonne Paris Cité, F-75019 Paris, France.
[19]Faculté de Médecine Denis Diderot, Univ Paris Diderot - Sorbonne Paris Cité, Paris, France.
[20]Département de Génétique, Hôpital Robert Debré, AP-HP, Paris, France.
[21]Service de Neuropédiatrie, Hôpital Robert Debré, AP-HP, Paris, France.
[22]Centre for the Developing Brain, Department of Division of Imaging Sciences and Biomedical Engineering, King's College London, King's Health Partners, St. Thomas' Hospital, London, SE1 7EH, United Kingdom.

[23]Department of Cell Biology, Microbiology, and Molecular Biology, College of Arts and Sciences, University of South Florida, Tampa, Florida, United States of America

[23]MRC Laboratory of Molecular Biology, Cambridge Biomedical, Campus, Cambridge, UK.

Present addresses :

bioRxiv preprint doi: https://doi.org/10.1101/481457; this version posted December 26, 2018. The copyright holder for this preprint (which was not certified by peer review) is the author/funder. All rights reserved. No reuse allowed without permission.

ψ Department of Molecular Biology and Genetics, Cornell University, Ithaca, NY 14853, USA
θ Department of Genetics and Evolution, Sciences III, University of Geneva, Geneva, Switzerland
ξ INRA, Nutrition et Neurobiologie Intégrée, UMR1286, Bordeaux, France
£ Université de Bordeaux, Nutrition et Neurobiologie Intégrée, UMR1286, Bordeaux, France

[&]Co-corresponding authors: aurelie.dethonel@univ-paris-diderot.fr; 33 (0)1 57 27 89 25. lea.sistonen@btk.fi; Tel: +358-2-2153311; Fax: +358-2-3338000; valerie.mezger@univ-paris-diderot.fr; Tel: 33 (0)1 57 27 89 14; 33 (0)6 75 77 11 98; Fax: 33 (0)1 57 27 89 11.
[§]Co-first authors: these authors contributed equally to the work.
*Co-last authors : these authors contributed equally to the direction of the work.

Acknowledgments: We warmly thank the patients and their families for their participation in this study. We thank Slimane AIT-SI-ALI for helpful discussions and comments on the manuscript, Anne PLESSIS (Jacques Monod Institute, Paris, France) for helpful discussions on setting the SNAP-TAG technology, Anne VANET (Jacques Monod Institute, Paris, France) for helpful discussions on the HSF2 structural modelling. We thank Lauriane FRITSCH and Slimane AIT-SI-ALI (UMR7216, for HeLa-S3 cells and growth conditions for TAP-TAG analyses). We thank the Imaging Platform IMAGOSEINE and especially N. BOGETTO for her help in sorting the GFP-positive HeLa-S3 cells. We are grateful to Heinrich LEONHARDT (Ludwig-Maximilians University, München, Germany) for F3H cellular and molecular tools and Pierre-Antoine DEFOSSEZ and Laure FERRY (UMR7216) for helpful guidance in F3H and GFP-Trap experiments, Isabelle LEMASSON (East Carolina University, USA) for the KIX-GST constructs, and Sophie POLO (UMR7216) for SNAP-TAG vectors. We thank Isabelle COUPRY and Benoit ARVEILER (CHU de Bordeaux, France) for primary skin fibroblasts from healthy donors. We thank the Institut Médical Jérôme Lejeune for the gift of Lymphoblastoid cells (patients 4 and 5). We are grateful to Delphine BOHL, and Stéphane BLANCHARD from Pasteur Institute (Rétrovirus et Transfert Génétique, INSERM U622) for their help in producing the retroviruses for TAP-TAG experiments in Hela-S3 cells. We thank Clara GIANFERMI (UMR7216) for microscopy pictures of organoids and nSBs. We thank Isabelle Le PARCO and the staff from the Buffon animal housing facility at the Jacques Monod Institute (Paris Diderot University, Paris, France) and the *Bioprofiler* Platform at the UMR8251 Biologie Fonctionnelle et Adaptative for *in vitro* acetylation assays.

Funding information :
VM was funded by the CNRS (Projet International de Coopération Scientifique PICS 2013-2015) for her collaboration with LS and by the Short Researcher Mobility France Embassy/MESRI-Finnish Society of Sciences and Letters; the Agence Nationale de la Recherche («NeuroHSF», Programme Neurosciences, Neurologie and Psychiatrie ANR-06-NEURO-024-01 and « HSF-EPISAME », SAMENTA ANR-13-SAMA-0008-01). LS was funded by the Academy of Finland, Sigrid Jusélius Foundation, Magnus Ehrnrooth Foundation and Cancer Foundation Finland.
RA was supported by PhD Fellowships from Neuropôle Ile-de France and Fondation ARC, FM by PhD Fellowships from the CNRS and Fondation pour la Recherche Médicale and from a Postdoc Fellowship from SAMENTA ANR-13-SAMA-0008-01), AD by a Ministère de l'Enseignement supérieur, de la Recherche et de l'Innovation (MESRI) Doctoral Fellowship, and ADT, DSD, and DB by the PICS travel grant, and GP and MH by Master 2 Intership Fellowships from SAMENTA ANR-13-SAMA-0008-01. JKA was supported by Magnus Ehrnrooth foundation. MCP was supported by the Turku Doctoral Network in Molecular Biosciences and Magnus Ehrnrooth Foundation. The supporting bodies played no role in any aspect of study design, analysis, interpretation or decision to publish this data.

bioRxiv preprint doi: https://doi.org/10.1101/481457; this version posted December 26, 2018. The copyright holder for this preprint (which was not certified by peer review) is the author/funder. All rights reserved. No reuse allowed without permission.

SUMMARY

Cells respond to protein-damaging insults by activating heat shock factors (HSFs), key transcription factors of proteostasis. Abnormal HSF protein levels occur in cancer and neurodegenerative disorders, highlighting the importance of the tight control of HSF expression. HSF2 is a short-lived protein, but it is abundant in the prenatal brain cortex and required for brain development. Here, we reveal that HSF2 is acetylated and co-localized with the lysine-acetyl transferases CBP and EP300 in human brain organoids. Using unbiased, biochemical, cell-imaging, and *in silico* approaches, we show that CBP/EP300 acetylates HSF2 at specific lysine residues, which promotes HSF2 stabilization, whereas the lysine deacetylase HDAC1 catalyzes its proteasomal degradation. The CBP KIX domain and KIX-recognizing motifs in HSF2 are critical for its interaction with acetylating enzymes. The functional importance of acetylated HSF2 is evidenced in Rubinstein-Taybi syndrome (RSTS), characterized by mutated CBP or EP300. We show that RSTS patient cells exhibit decreased HSF2 levels and impaired heat shock response. The dysregulated HSF pathway in RSTS opens new avenues for understanding the molecular basis of this multifaceted pathology.

bioRxiv preprint doi: https://doi.org/10.1101/481457; this version posted December 26, 2018. The copyright holder for this preprint (which was not certified by peer review) is the author/funder. All rights reserved. No reuse allowed without permission.

INTRODUCTION

Since their discovery three decades ago, our way to envision the regulation and roles of the Heat Shock transcription Factor family (HSFs) has been revolutionized. Originally identified and characterized due to their stress-responsiveness and ability to recognize a consensus DNA-binding site, the heat shock element (HSE), HSFs were more recently shown to perform an unanticipated large spectrum of roles under physiological and pathological conditions (Wu, 1995; Abane and Mezger 2010; Akerfelt et al., 2010; Pastor-Gomez et al., 2018). HSFs are activated by a diversity of stressors that provoke protein damage and govern the highly conserved Heat Shock Response (HSR). The HSR contributes to the restoration of proteostasis, through the regulation of genes encoding molecular chaperones, including the Heat Shock Proteins (HSPs; Hartl et al., 2011). HSFs also control immune/inflammatory pathways, metabolism, and, through dysregulation of their protein levels or activity, shape disease susceptibility to cancer, metabolic and neurodegenerative disorders. These pathophysiological roles are performed through altered expression of a broad repertoire of target genes, beyond the *HSPs* (Xiao et al., 1999; Inouye et al., 2007; Dai et al., 2007; Mendillo et al., 2012; Santagata et al., 2013; Anckar and Sistonen, 2011; Jin et al., 2011; Neef et al., 2011; Nakai, 2016; Pastor-Gomez et al., 2017 and 2018). The multifaceted roles of HSFs are achieved by their fascinating plasticity in terms of multi-modular structure and assembly of homo- or heterodimers or trimers, stress- and context-dependent posttranslational modifications as well as a diversity of partner networks. As a consequence, HSFs act as fine sculptors of transcriptomic and epigenetic landscapes, through dynamic interactions with other transcriptional activators or repressors and chromatin remodelling complexes (Akerfelt et al., 2010; Miozzo et al., 2015; Pastor-Gomez et al., 2018; Raychaudhuri et al. 2014).

The versatile functions of HSFs have been mostly studied with HSF1 and HSF2, two members of the mammalian HSF family, which in human comprises four additional members, i.e. HSF4, HSF5, HSFX and HSFY (Pastor-Gomez et al., 2018). The role of HSF1 in acute and severe proteotoxic stress, including exposures to elevated temperatures (42-45°C), has been extensively documented and become a paradigm for the *modus operandi* of the HSF family. In contrast, HSF2 appears to be responsive to stresses of relevance for chronic or pathological situations, such as fever-like temperatures at 39-41°C (Shinkawa et al., 2011), alcohol (ethanol) exposure (El Fatimy et al., 2014; Miozzo et al., 2018), and prolonged proteasome inhibition (Lecomte et al., 2010; Rossi et al., 2014). Both factors have been involved in cancer, in a dual manner. HSF1 acts as a potent, multifaceted facilitator of cancer initiation and progression (Dai et al., 2007; Mendillo et al., 2012; Santagata et al., 2013), whereas HSF2 expression can ensure a protective role, by counteracting tumor progression and invasiveness (Björk et al. 2016). The control of HSF1 protein levels is key for its role in cancer, and elevated HSF1 expression is associated with poor prognosis (Santagata et al., 2011) while its decreased expression is associated with neurodegenerative disorders (Kim et al., 2015; Jiang et al., 2013; Pastor-Gomez et al., 2017; reviewed in Pastor-Gomez et al., 2018). HSF1 and HSF2 are also important players in the physiological brain development and adult brain integrity. Furthermore, we and others have shown that the deregulation of HSF activities underlies neurodevelopmental defects (Kallio et al., 2002; Wang et al., 2003; Chang et al., 2006; El Fatimy et al., 2014; Hashimoto-Torii et al., 2014; Ishii et al., 2017; reviewed in Abane et Mezger 2010, Akerfelt et al., 2010, Pastor-Gomez et al., 2018) and neurodegenerative processes (Shinkawa et al., 2011; Pastor-Gomez et al., 2017). The complexity of the role of HSF2 and its impact on pathophysiological situations, including cancer, neurodevelopmental and neurodegenerative diseases, thus raises questions about the regulatory mechanisms of HSF2 expression.

The amount of the HSF2 protein varies in diverse cellular or embryonic contexts and conditions: both transcriptional and post-transcriptional mechanisms have been indicated to regulate *HSF2* mRNA levels (Rallu et al., 1997; Björk et al., 2010). In the developing brain, the amount of HSF2 protein seems to correlate with that of *Hsf2* transcripts, underlining the importance of transcriptional control

bioRxiv preprint doi: https://doi.org/10.1101/481457; this version posted December 26, 2018. The copyright holder for this preprint (which was not certified by peer review) is the author/funder. All rights reserved. No reuse allowed without permission.

(Rallu et al., 1997; Kallio et al., 2002; Wang et al., 2003). Moreover, HSF2 is a short-lived protein and its stabilization constitutes an important step controlling its DNA-binding activity (Sarge et al., 1993; Mathew et al., 1998; Kawazoe et al., 1998) and mediating its role in physiological processes and stress responses. HSF2 protein levels also fluctuate during the cell cycle and its stabilization is an important control step in fine-tuning the HSR (Elsing et al., 2014). Indeed, HSF2 modulates the stress-inducible expression of *HSP* genes, which is primarily driven by HSF1 (Östling et al., 2007). This transient modulatory function of HSF2 is due to the rapid poly-ubiquitination and proteasomal degradation in response to acute heat stress (Ahlskog et al., 2010). While diverse posttranslational modifications (PTMs), such as phosphorylation and acetylation, are known to control HSF1 stability (Kourtis et al., 2015; Pastor-Gomez et al., 2017; Raychaudhuri et al., 2014; reviewed in Pastor-Gomez et al., 2018), the mechanisms regulating stability of HSF2 are not well understood, and given its role in chronic stress, cancer, and physiopathological developmental processes, they are crucial to be elucidated.

In this study, using both candidate and unbiased approaches, we demonstrate a specific role for acetylation in controlling HSF2 stability, under normal growth and stress conditions. We identify the histone/lysine-acetyl transferases (HATs/KATs) CBP (CREB-binding protein; KAT3A) and EP300 (KAT3B) as key enzymes to catalyze HSF2 acetylation. We show that HSF2 is acetylated during normal brain development in human organoids and mouse cortices, where it co-localizes with CBP and EP300. We identify three main HSF2 lysine residues, whose acetylation by CBP/EP300 is critical for its stability. In contrast, HDAC1 that we identify as an HSF2 partner, by TAP-TAG and mass spectrometry, promotes HSF2-proteasomal degradation. We identify the KIX-recognition motifs in the HSF2 oligomerization domain and show that they are key for interaction with the KIX domain of the CBP protein. We also demonstrate the functional impact of HSF2 acetylation and stabilization by CBP/EP300, in a rare disease the Rubinstein-Taybi syndrome (RSTS; Lopez-Atalaya et al., 2014; Spena et al., 2015a). RSTS is characterized by mutations in the *CREBBP* (*CBP*; RSTS1, OMIM #180849*)* or *EP300* (RSTS2; OMIM #613684) genes, with multiple congenital anomalies, neurodevelopmental defects, childhood cancer susceptibility, and vulnerability to infections. We observe that cells derived from RSTS patients exhibit marked destabilization of the HSF2 protein, which is rescued by proteasomal inhibition. These cells also display altered basal expression of HSPs and impaired HSR. The disruption of the HSF pathway in RSTS highlights the importance of the CBP/EP300 dependent regulation of HSF2 by acetylation and provides a new conceptual frame for understanding the molecular basis of this complex and multifaceted pathology.

bioRxiv preprint doi: https://doi.org/10.1101/481457; this version posted December 26, 2018. The copyright holder for this preprint (which was not certified by peer review) is the author/funder. All rights reserved. No reuse allowed without permission.

RESULTS

HSF2 is acetylated and interacts with CBP/EP300 in the developing brain

The levels of the HSF2 protein are highly variable among cell types and organs (Abane and Mezger, 2010). In particular, HSF2 is remarkably abundant in the vertebrate developing brain, where it exhibits spontaneous DNA-binding activity, in normal non-stressed conditions (Rallu et al., 1997; Kawazoe et al. 1999; Kallio et al., 2002; Wang et al., 2003; Chang et al., 2006). As a first step to determine whether HSF2 acetylation was involved in controlling HSF2 stability similarly to HSF1 acetylation by EP300 (Raychaudhuri et al., 2014), we compared HSF2 and CBP/EP300 expression profiles, and investigated whether HSF2 acetylation could be detected in the developing mammalian cortex under physiological conditions. Indeed, CBP and EP300 are transcriptional coactivators that interact with a large number of transcription factors (TFs) and have key roles in neurodevelopment (reviewed in Chan and La Thangue 2001; Lopez-Atalaya et al., 2014).

To the best of our knowledge, the expression of the HSF2 protein in the human developing cortex has not been reported. By generating brain organoids from human induced pluripotent stem cells (iPSCs; Lancaster et al., 2014), we found that HSF2 was expressed at different stages, from day 20 (embryoid bodies) to day 60 of differentiation (D20 – D60), as shown in mRNA and protein analyses (Figure 1A and S1A). By immunofluorescence on D60 organoids, we found that HSF2 was expressed in neural progenitor cells (NPCs; located in areas of dense DAPI-staining, as verified by SOX2 staining, Figure S1B) and in neurons, expressing beta-III tubulin, in regions displaying a cortical-like morphology (Figure 1B and S1B). In addition, we observed co-labeling of EP300 and HSF2 in NPCs (arrowheads) and neurons (arrows) (Figure 1C). Thus, HSF2 and EP300 (also CBP; see Figure S1C) thus exhibited similar expression territories (NPCs and neurons; Figure S1B,C). In addition, HSF2, CBP and EP300 were expressed, in a concomitant manner, in the mouse cortex from E11 to E17 (Figure S1D; note that CBP and EP300 expression patterns have been previously reported in the mouse embryonic brain, mostly at early stages; Kawasaki et al. 1998; Yao et al., 1998; Partanen et al., 1999; Bhattacherjee et al; 2009). The similarity of their expression patterns supported a possible interaction between HSF2 and the CBP and EP300 in the developing cortex. Accordingly, HSF2 was co-immunoprecipitated with CBP and EP300 (Figure 1D and Figure S1E, left panels). We also detected acetylated HSF2 in the developing mouse cortex (Figure 1E and Figure S1E, right panels) and in D40 human brain organoids (Figure 1F). Similarly, HSF2 was found acetylated in SHSY-5Y neuroblastoma cells, a human cancer cell line of neural origin (Figure S1F). Altogether, these results show that, HSF2 is acetylated and interacts with CBP and EP300 in the developing brain.

Analysis of CBP/EP300-mediated HSF2 acetylation in mammalian cell lines

In order to explore the mechanism and function of HSF2 acetylation, we first verified whether HSF2 was a novel substrate for acetylation by CBP/EP300, in human in HEK 293 cells, co-expressing CBP-HA or EP300-HA and tagged HSF2. Using GFP- or Myc-Trap (Rothbauer et al., 2008) assay, we found that the immunoprecipitated exogenous HSF2-YFP or HSF2-Myc protein was acetylated by EP300 or CBP (Figure 2A) and that no acetylation was observed in cells transfected by dominant-negative CBP (Figure 2B).

To identify the acetylated lysine residues in HSF2, we co-expressed Flag-HSF2 with EP300-HA in HEK 293 cells. HSF2 was immunoprecipitated and the acetylation of lysines was detected by mass spectrometry (MS). Among the 36 lysine residues of HSF2, we identified eight acetylated lysines: K82, K128, K135, K197, K209, K210, K395, and K401 (Figure 2C, Figure S2A, and Table S1). Single point mutations (K82, K128, K135, and K197), or mutation of the doublet K209/K210 (Figure S2B) to arginine (R), which prevent acetylation, did not abolish HSF2 acetylation, suggesting that, in line with our MS data, the acetylation of HSF2 occurs on more than one lysine residue. Indeed, the mutation to either arginine (R) or glutamine (Q) of three or four lysines (K82, K128, K135 and K197), located within the DNA-binding domain and the first hydrophobic heptad repeat (HR-A/B), dramatically reduced HSF2 acetylation (Figure 2D and Figure S2C). Using an *in vitro* acetylation assay coupled with HPLC, we found that synthetic HSF2 peptides containing K135 and K197 residues were readily acetylated by recombinant purified CBP-HA, in an acetyl-CoA-dependent manner (Figure 2E and

bioRxiv preprint doi: https://doi.org/10.1101/481457; this version posted December 26, 2018. The copyright holder for this preprint (which was not certified by peer review) is the author/funder. All rights reserved. No reuse allowed without permission.

Figure S2D-F), but not a peptide containing the K82 lysine. Note that we could not perform this experiment on the HSF2 peptide containing K128, due to its insolubility. Taken together, our data suggest that HSF2 is acetylated by CBP/EP300 at three major lysine residues, residing in the HR-A/B domain: K128, K135 and K197.

Interaction of HSF2 with the core catalytic domain of CBP

Prompted by the finding that a catalytically active CBP is necessary for HSF2 acetylation, we examined whether HSF2 could bind to the core catalytic domain of CBP. The CBP central core catalytic region ("Full-HAT"; Figure 3A) contains the Bromodomain BD, the cysteine/histidine-rich region CH2, and the HAT domain and allows the coupling of substrate recognition and histone/lysine acetyltransferase (HAT) activity (as in EP300; Delvecchio et al., 2013; Dancy and Cole, 2015; Dyson and Wright 2016). The CH2, in particular, contains a RING domain and the PHD (plant homeodomain, a non-canonical zinc finger; Park et al., 2013). With Biolayer interferometry, we observed that the recombinant Full-HAT domain directly interacted with immobilized biotinylated recombinant full-length HSF2 (Figure 3B). Within this region, the recombinant PHD domain, but not the HAT, RING or BD domain, was able to interact with HSF2, in a similar manner as the "Full-HAT" domain (Figure 3B). Interestingly, the interaction of HSF2 with the Full-HAT or the PHD domain was more efficient than with HSP70, which has been reported to interact with HSF2 (Huttlin et al., 2015; Tang et al., 2016). As expected, it is likely that the interaction between HSF2 and the catalytic HAT domain was too transient to be captured in these experiments, because the structural integrity of the HAT domain is dependent on the BD and CH2 domains. The latter includes the PHD domain which is involved in protein interaction and in the case of CBP is considered an integral part of the enzymatic core HAT domain, being critical for HAT activity (Aasland et al., 1995; Bordoli et al., 2001; Kalkhoven et al, 2002). We determined that the K_D of HSF2 interaction with the CBP Full-HAT domain was $1.003E^{-09}$ M (+/-$2.343E^{-11}$; R2= 0.988488; Figure S3A). The interaction of HSF2 with the Full-HAT domain, and the PHD within, together with our data on HSF2 acetylation strongly suggest that HSF2 is a *bona fide* substrate of CBP, and potentially of EP300 since their HAT domains display 86% identity.

HSF2 interacts with CBP and EP300 *in cellulo*

Next we investigated whether HSF2 can interact with CBP or EP300 *in cellulo*. Using HEK 293 cells in GFP-Trap assay, we showed that CBP-HA or EP300-HA co-immunoprecipitated with HSF2-YFP (Figure 3C,D). We also observed that endogenous CBP and EP300 co-precipitated with endogenous HSF2 in the murine neuroblastoma N2A cells (Figure S3B). We confirmed these interactions by an independent technique, the fluorescent three-hybrid assay (F3H; Figure 3E-G; Herce et al., 2013), using GFP-binder and HSF2-YFP, together with CBP-HA or EP300-HA. In negative control experiments, GFP-binder, which was recruited to the *LacOp* array locus, was unable to recruit endogenous CBP, CBP-HA, or EP300-HA (Figure S3C-E). Similarly, HSF2-YFP was unable to locate at the *LacOp* array locus in the absence of GFP-binder (Figure S3C-E). Co-transfection of HSF2-YFP with CBP-HA or EP300-HA resulted in the formation of a red spot in the nucleus, showing co-recruitment to the HSF2-YFP focus, in 68.4 % and 48.6 % of the cells, respectively (Figure 3F, upper panels and 3G). The abundance of CBP in the BHK cells allowed us to detect the co-recruitment of HSF2-YFP with endogenous CBP in 43.9% of these cells (Figure 3F, lower panels).

The HR-A/B domain of HSF2 is key for interaction with CBP and acetylation.

To determine which HSF2 domains were important for its interaction with CBP, we expressed Flag-HSF2, either full-length or deletion mutants of different domains, in HEK 293 cells. The deletion mutants of different domains, we showed that the deletion of HR-A/B (or DBD plus HR-A/B, but not DBD only) led to a marked decrease in HSF2 acetylation (Figure S4A-C; see red arrow) and interaction with CBP (Figure S4D). These results were in line with our findings that the major acetylated lysine residues reside within the HR-A/B domain. The deletion of the TAD (transcription activation domain; Jaeger et al., 2016) also resulted in decreased acetylation of the Flag-HSF2 (Figure S4B-C) and was

bioRxiv preprint doi: https://doi.org/10.1101/481457; this version posted December 26, 2018. The copyright holder for this preprint (which was not certified by peer review) is the author/funder. All rights reserved. No reuse allowed without permission.

associated with decreased interaction with CBP (Figure S4D). This domain may also be important for interaction between CBP and HSF2, since the multivalent interactions between CBP/EP300 and many TFs generally involve their TADs (Lee et al., 2009; Wang et al., 2012; reviewed in Thakur *et al*., 2013).

The presence of KIX motifs in the HSF2 HR-A/B domain promotes binding to the CBP KIX domain

The interaction between HSF2 and the core catalytic domain is likely facilitated/stabilized *via* specific domains of these two proteins. CBP/EP300 interacts with many transcription factors *via* different binding sites, including the KIX domain (kinase-inducible domain interacting domain; Figure 3A, left). The KIX domain contains two distinct binding sites that are able to recognize the "ΦXXΦΦ" KIX motif, where "Φ" is a hydrophobic residue, and "X" is any amino acid residue (Radhakrishnan et al., 1997; Kobayashi et al., 1997; Lee et al., 2009; Zor et al., 2004). Importantly, we found that the HR-A/B domain of HSF2 contains several conserved, overlapping and juxtaposed KIX motifs (Figure 4A). We verified, using recombinant proteins that HSF2 was co-immunoprecipitated with the CBP KIX domain, in *in vitro* GST-pull-down experiments (Figure 4B). We then modeled the interaction between the HSF2 HR-A/B KIX motifs and the CBP KIX domain. Based on sequence similarities between the HR-A/B domain, lipoprotein Lpp56, and the transcription factors GCN4, ATF2, and PTRF (Figure S4E; see Experimental procedures), we first developed a structural model of the HSF2 trimeric, triple coiled-coil, HR-A/B domain (Jaeger et al., 2016). Next, we evaluated the possibility of interactions of the KIX recognition motifs in the HR-A/B region with the CBP KIX domain. Best poses suggested that the HR-A/B KIX motif region contacted the c-Myb surface (Figure 4C), thereby proposing a close interaction of the HSF2 KIX motifs with tyrosine Y650 (Figure 4D). We assessed the impact of *in silico* mutations of the Y650 amino-acid of the CBP KIX domain or K177, K180, F181, V183 residues in the HSF2 KIX motifs, involved in the contact with CBP (Figure 4E). Interestingly, the *in silico* mutation of CBP residue Y650A profoundly decreased the probability of interaction of the HSF2 KIX motifs with the KIX domain (Figure 4F, upper panel; and Figure S4F (b). We also found that the Y650A mutation disrupted HSF2 and KIX interaction, in GST-pull-down experiments (Figure 4F, lower panel). Interestingly, this mutation has been identified in RSTS, and associated with a severe neurodevelopmental phenotype (Spena et al., 2015b). In addition and in constrast to F181A or V183A mutation (Figure S4F (c,d)), the K177A or Q180A mutation within the HSF2 KIX motifs also disrupted HSF2-KIX interaction (Figure S4F (e,f)), highlighting the importance of these residues in these interactions

The acetylation of HSF2 governs its stability in non-stress conditions

We then explored the functional impact of the CBP/EP300-mediated acetylation of HSF2. Endogenous HSF2 protein levels were decreased upon pharmacological inhibition of CBP/p300 activity in N2A cells, using the specific inhibitor C646 (Bowers et al., 2010; Dancy and Cole, 2015; Figure 5A and Figure S5A). This decrease was abolished by treatment with the proteasome inhibitor, MG132, suggesting that the decrease in the HSF2 protein levels was dependent on the proteasomal activity, and that HSF2 was degraded when CBP/EP300 activity was inhibited (Figure 5A). This observation provided the first evidence for acetylation playing a regulatory role in HSF2 stability. To further investigate the role of acetylation in the regulation of HSF2 protein levels, we generated CRISPR/Cas9 *Hsf2*KO U2OS cell lines (2KO; Figure S5B-F) and measured the protein levels of wild type HSF2 and HSF2 acetylation mutants, which mimic either constitutively acetylated (3KQ) or non-acetylated (3KR) HSF2 (Figure 5B-D). We first verified that the HSF2 WT, and HSF2 3KQ and HSF2 3KR were expressed at comparable levels (Figure S5D), and capable of binding DNA in *in vitro* and its binding sites on repeated pericentromeric *Satellite III* DNA (*Sat III*), *in ex vivo* experiments (Figure S5E,F). To monitor the decay of a pre-existing pool of HSF2 molecules, we performed pulse-chase experiments using the SNAP-TAG technology (Bodor et al., 2012). A pool of SNAP-HSF2 molecules was covalently labeled by adding a fluorescent substrate to the cells. At t_0, a blocking non-fluorescent substrate was added, quenching the incorporation of the fluorescent substrate to newly synthesized HSF2 molecules (Figure 5B), allowing us to measure the decay in the fluorescence intensity of the corresponding labeled HSF2 bands. When 2KO cells were transfected with wild-type SNAP-HSF2

bioRxiv preprint doi: https://doi.org/10.1101/481457; this version posted December 26, 2018. The copyright holder for this preprint (which was not certified by peer review) is the author/funder. All rights reserved. No reuse allowed without permission.

(SNAP-HSF2 WT), the decay in fluorescence intensity of the corresponding bands was observed within 5 hours (Figure 5C and D). Preventing HSF2 acetylation in cells transfected with SNAP-HSF2 3KR resulted in a similar decay (Figure 5C and D). In contrast, mimicking acetylation in cells expressing SNAP-HSF2 3KQ protected HSF2 from decay (Figure 5C and D). Importantly, proteasome inhibition with MG132, prevented the decrease in SNAP-HSF2 WT and SNAP-HSF2 3KR fluorescent intensity, strongly suggesting that HSF2 decay was dependent on the proteasomal activity (Figure 5E).

HDAC1/2 is involved in destabilization of the HSF2 protein under non-stress and stress conditions

To identify the enzymes that could function as deacetylases for HSF2, we performed an unbiased screen for HSF2 binding partners, using a double-affinity TAP-TAG approach (Bürkstümmer et al., 2006; Figure S6A-C). For this purpose, we generated a HeLa-S3 cell line expressing double-tagged HSF2 (or transfected with the empty vector as a negative control) and analyzed nuclear extracts by MS. We identified HDAC1 as one of the protein partners of HSF2 (Figure 6A). In addition to HSF2, we found nucleoporin Nup62 (Figure 6A), an earlier identified HSF2 partner that provided a positive control for the quality of our TAP-TAG/MS analysis (Yoshima et al., 1997). We also performed immunoprecipitation of HSF2 in extracts from the mouse E17 cortices, a stage at which HSF2 protein levels are decreased (see Figure S1D), followed by MS analysis. We identified both HDAC1 and HDAC2 as HSF2 partners (Figure S6D). Using the F3H approach (Figure 6B and Figure S6E), and co-immunoprecipitation in GFP-Trap assays (Figure 6C), we confirmed the interaction between HSF2 and HDAC1 in mammalian cell lines. We then observed that preventing the acetylation of HSF2 by expressing Myc-HSF2 3KR increased the polyubiquitination of HSF2, compared to HSF2 WT or HSF2 3KQ (Figure 6D). For evaluating the impact of HDAC1 and other Class I HDACs on the acetylation of HSF2, we expressed tagged HDAC1, HDAC2, HDAC3, or HDAC8, concomitantly with CBP-HA and Flag-HSF2 in HEK 293 cells (Figures 6E and S6F). HDAC1 overexpression resulted in marked reduction in HSF2 acetylation levels, whereas HDAC2 and HDAC3 had only limited effects, and HDAC8 no obvious impact (Figures 6E and S6F).

Because heat shock (HS) provokes the degradation of the HSF2 (Ahlskog et al., 2010), we also examined the role of acetylation on the turnover of the HSF2 protein upon HS. The impact of acetylation on the decay of HSF2 upon HS analyzed using the SNAP-TAG technology. Mimicking the acetylation of the three major acetylated lysine residues mitigated the decay of fluorescence intensity of SNAP-HSF2 3KQ induced by HS, compared to SNAP-HSF2 WT or 3KR (Figure 6F). The impact of HDAC inhibition on endogenous HSF2 was investigated in neural N2A cells. We first verified that HS induced decay in HSF2 protein levels also in neural N2A cells, although it occurred at a slower rate (Figure S6G) when compared to HeLa or HEK 293 cells (Ahlskog et al., 2010). Treatment with 1 mM of the Class I inhibitor VPA dampened the decline in HSF2 protein levels in N2A cells upon HS (Figure 6G). This suggested that Class I HDAC activity participates to the degradation of HSF2 upon HS, likely through HSF2 deacetylation (Figure 6G). We then verified that HS increased HSF2 polyubiquitination in HEK293 cells, as previously reported (Ahlskog et al. 2010; Figure 6H, Mock). To investigate whether HDAC1 could favor HSF2 polyubiquitination, likely through HSF2 deacetylation, we examined the impact of overexpression of a dominant-negative form of HDAC1 on HSF2 ubiquitination. We showed that, indeed, the increase in HSF2 polyubiquitination upon HS was mitigated in HEK 293 cells transfected with dominant-negative HDAC1 (Figure 6H). Altogether, these results support a role of HDAC1 (and possibly other Class I HDACs) in the destabilization of HSF2 under normal and stress conditions, through HSF2 polyubiquitination and proteasomal degradation.
In summary, the acetylation status of HSF2 thus appears to play a key role for the stabilization of the HSF2 protein, by protecting it from proteasomal degradation.

Declined HSF2 protein levels in the Rubinstein-Taybi Syndrome (RSTS)

To evaluate the impact of CBP and EP300 on HSF2 levels, in a pathological context, we compared the amounts of HSF2 protein in cells derived from either healthy donors (HD) or RSTS patients, which are characterized by autosomal-dominant (heterozygous) mutations in the *CBP* or

bioRxiv preprint doi: https://doi.org/10.1101/481457; this version posted December 26, 2018. The copyright holder for this preprint (which was not certified by peer review) is the author/funder. All rights reserved. No reuse allowed without permission.

EP300 genes, leading to neurodevelopmental defects and intellectual disabilities (see Figure S7A for a description of the mutations). We used human primary skin fibroblasts (hPSFs), at early passages (see Experimental Procedures), to avoid the putative compensation processes during *ex vivo* culture. We observed that HSF2 protein levels were markedly decreased in RSTS patients mutated in either *CBP* or *EP300* ($RSTS_{CBP}$, patient 1 [P1] and $RSTS_{EP300}$, patient 2 [P2]; Figure 7A-C). These levels were restored to the levels that are comparable in healthy donors (HD) when hPSFs had been treated with the proteasome inhibitor MG132 (Figure 7A and B). Note that we verified the impact of *CBP* or *EP300* mutations in RSTS hPSFs, by showing that the amount of acetylated lysine residue K27 in histone H3 (AcH3K27) was reduced in both cases (Figure 7A and C; right panels). Interestingly, Class I HDAC inhibition by VPA could not restore HSF2 levels in $RSTS_{CBP}$ or $RSTS_{EP300}$ hPSFs, although HD and RSTS cells displayed similar levels of HDAC1 (Figure S7D). This suggests that, in RSTS hPSFs, CBP and EP300 are key for the stabilization of HSF2 (Figure 7A; Figure S7B). Notably, the stability of HSF2 was impaired both in the $RSTS_{CBP}$ patient carrying a mutation in the catalytic domain of CBP and in the $RSTS_{EP300}$ patient carrying a deletion of the KIX domain of EP300, which was shown to be a binding site for HSF2 as shown by our results (Figure 4C). This suggests that both domains are required for the regulation of HSF2 stability, in line with our results (Figure 3 and 4). Altogether these results demonstrate that the proteasomal turnover of HSF2 is increased in RSTS hPSFs, carrying mutated *EP300* or *CBP*, thereby strongly suggesting that EP300 and CBP are key regulators of HSF2 protein stability.

Impaired heat shock response in RSTS cells

HSF1 is the essential driver of the acute heat shock response (HSR) in mammals (McMillan et al., 1998). Although dispensable for the HSR in most cellular contexts (McMillan et al., 1998), HSF2 acts as a fine tuner of the HSR (Östling et al., 2007; Elsing et al., 2014), which governs the magnitude to which HS induces *HSP* gene expression. Therefore, we evaluated the ability of RSTS cells to mount a HSR. In the absence of heat stress, we observed that RSTS hPSFs displayed lower amounts of HSP70 and HSP90 than HD counterparts (Figure 7D). Furthermore, $RSTS_{EP300}$ hPSFs exhibited limited capacity in inducing HSP70 accumulation upon HS and during the recovery phase from heat stress (Figure 7D). Notably, this limited induction did not result from impairment of HSF1 activation, since HSF1 seemed activated by HS in $RSTS_{EP300}$ hPSFs, as assessed by its mobility shift in SDS-PAGE (see arrow head and arrow in Figure 7D). This shift is a hallmark of HSF1 hyperphosphorylation, which, although not required for HSF1 activation, accompanies the induction of HSF1 transactivation potential (Sarge et al., 1993; Budzyński et al., 2015; reviewed in Anckar and Sistonen, 2011;). HSF1 and HSF2 do not only control the transcription of the *Hsp* genes, but they also upregulate the transcription of *Sat III* (*Sat III*) pericentromeric heterochromatin regions, in response to acute heat stress. This process results in the accumulation of non-coding RNAs, predominantly at the *SatIII* 9q12 locus, which participates to the formation of specific subnuclear structures, called the nuclear stress bodies (nSBs; Jolly et al, 1997, 1999, 2004; Rizzi et al., 2004; Sandqvist et al., 2009). We therefore used nSBs as read-out for the HSR integrity in RSTS cells and observed that the stress-inducible formation of nSBs was reduced by more than 50% in RSTS $_{EP300}$ hPSFs when compared to their HD counterparts (Figure 7E). A similar reduction in the formation of nSBs was observed in $RSTS_{EP300}$ or $RSTS_{CBP}$ lymphoblastoid cells (LBs; Figure S7F).

bioRxiv preprint doi: https://doi.org/10.1101/481457; this version posted December 26, 2018. The copyright holder for this preprint (which was not certified by peer review) is the author/funder. All rights reserved. No reuse allowed without permission.

DISCUSSION

HSFs exert a wide spectrum of key pathophysiological roles, whose unravelling has aroused an exciting wave of reawakened interest during the last decade and emphasized the importance of the tight control of HSF protein levels: excessive or insufficient HSF expression favors the development or progression of devastating diseases, including cancer, neurodevelopmental, and neurodegenerative disorders.

In this study, we have unraveled a novel mechanism that regulates the stability of the labile HSF2 protein, in different cellular contexts: the KATs CBP and EP300, control the acetylation of three highly conserved lysine residues K128, K135, and K197, located in the HR-A/B oligomerization domain, which are mainly responsible for HSF2 acetylation, and thereby contribute to the stability of the HSF2 protein. Moreover, we demonstrate the importance of this regulation which operates both in normal and stress conditions, in the pathological conditions of a rare disease.

HSF2 is acetylated by CBP/EP300 in various contexts including brain development

Based on our analysis, HSF2 is acetylated by the overexpression CBP or EP300 in cell systems. Moreover, we observe the acetylation of the endogenous HSF2 protein in human and murine neural embryonic tissues and cell lines (Figure 1 and S1), showing that HSF2 acetylation is not restricted to one specific cell context. CBP and EP300 and, more generally, HATs play significant roles during neurodevelopment (reviewed by Lopez-Atalaya et al., 2014). HSF2, CBP and EP300 exhibit very similar expression patterns along the organoid differentiation of human brain organoids, as they do in the developing mouse cortex. This is, to our knowledge, the first assessment of the expression profiles of HSF2, CBP, and EP300 in such models of the developing human brain and of interactions between HSF2 and CBP/EP300. These results point out the putative importance of HSF2 acetylation in physiological contexts and suggesting that the acetylation of HSF2 might participate to its high levels of expression and putatively role in cortical development. In line with this, note that we identified HDAC1 by MS analysis as an HSF2 partner in E17 cortices, a stage at which the HSF2 protein levels are markedly lowered (Figure S7; Rallu et al., 1997; El Fatimy et al., 2014).

Mode of HSF2 interaction with CBP/EP300

Endogenous or exogenous HSF2 interacts with CBP and EP300 in cell systems and in the developing brain cortex, as mentioned above. Our study unravels domains important for HSF2 acetylation *per se*, and for the anchorage of HSF2 to CBP/EP300. First, the full-length HSF2 protein interacts with the CBP core catalytic domain *in vitro*, confirming that HSF2 is a *bona fide* substrate of CBP. Interestingly, HSF2 also strongly interacts with the PHD domain, located in the catalytic core of the CBP/EP300 proteins (Delvecchio et al., 2013). Interestingly, mutations in the PHD domain have been identified in RSTS patients (Kalkhoven et al., 2003).

Second, we find that the HR-A/B oligomerization domain, but not the DBD, is necessary for HSF2 interaction with CBP and acetylation. We show that the HR-A/B domain specifically interacts with the KIX domain of CBP/EP300 in *in silico* analysis.

The KIX domain present in CBP and EP300 serves as a docking site for the binding of many transcription factors (TFs) that contributes to the properties of CBP/EP300 to act as a molecular bridge, stabilizing the interactions between TFs and the transcription apparatus (Parker et al., 1996; reviewed in Thakur et al., 2014). We find that the HR-A/B oligomerization domain contains a series of KIX-binding motifs that are necessary for HSF2 interaction with CBP and HSF2 acetylation. We show that these motifs specifically interact with the KIX domain of CBP/EP300 by *in silico* analysis. The *in silico* analyses indicate that the HR-A/B KIX motifs in HSF2 bind to the c-Myb site of the KIX domain. Indeed, the CBP or EP300 KIX domain can simultaneously - and in a cooperative manner - binds two polypeptide ligands, on two distinct surfaces, which have been historically called the “c-Myb” and the “MLL” (*Mixed Lineage Leukemia* protein) sites (reviewed in Thakur et al., 2014). For example, the activation domains of MLL and CREB, MLL and c-Myb, or Jun and CREB, can concomitantly bind to KIX, each TF contacting a different KIX surface, namely, the c-Myb or the MLL site (Goto et al., 2002;

bioRxiv preprint doi: https://doi.org/10.1101/481457; this version posted December 26, 2018. The copyright holder for this preprint (which was not certified by peer review) is the author/funder. All rights reserved. No reuse allowed without permission.

Campbell and Lumb, 2002). This suggests that the binding of another TF via the "MLL site" might potentially modulate HSF2 and CBP interaction, via the KIX domain.
In support of the close interaction between the HSF2 KIX recognition motifs and the CBP KIX domain, we show that the mutation of the tyrosine residue Y650 in the CBP KIX domain, which contacts the HSF2 KIX motifs, disrupts HSF2-CBP interaction in *in silico* and *in vitro* experiments.

We also identify the HSF2 TAD (Jaeger et al., 2016) as potentially important for HSF2 interaction with CBP. This result is reminiscent of other TF TADs that bind the KIX domain (reviewed in Thakur et al., 2014). Moreover, two different domains of the same TF (like p53 or FOXO3a; Lee et al., 2009; Wang et al., 2012) can simultaneously bind the KIX domain. It renders possible that HSF2 could simultaneously interact with CBP (and most likely EP300), through two distinct domains, the HR-A/B and the TAD domains. In addition, the di- or trimeric coil-coiled structure of HSF2 might also broadens the possibility of establishing multiple contacts with CBP, through KIX or other CBP domains, known to interact also with TADs, which paves the way for future studies.

The KIX domain of CBP/EP300 has a key role in the formation and stabilization of vital multi-protein complexes during transcriptional activation. Our data mining on two data sets generated in K562 cells: our HSF2 ChIP-Seq data (Vihervaara et al., 2013) and publically available EP300 ChIP-Seq data (*ENCODE UCSC Accession*: wgEncodeEH002834)) indicate that HSF2 and EP300 share common binding regions on the genome (data not shown), including two known HSF2 target genes: *HSP70* and *UBB.* We have already validated *UBB* as an HSF2 target gene in K562 cells (Vihervaara et al., 2013) and EP300 is recruited to *HSP70B*, in stress and brain development contexts (Xu et al., 2008; Marinova et al., 2009; Westerheide et al., 2009; Takii et al., 2014). This suggests that the interaction of HSF2 and CBP/EP300, which is important for the acetylation and stabilization of HSF2, can also occur on DNA, and might also contribute to the sculpting of the epigenetic and transcriptomic landscape of HSF2 target genes.

Dynamics of HSF2 acetylation by CBP/EP300, deacetylation by HDAC1, and degradation

Based on our data, the acetylation of HSF2 by CBP/EP300 limits its proteasomal degradation, as it does for other TFs, like p53, STAT3, or HIF1alpha (Grossman, 2001; Jain et al., 2012; reviewed in Yang and Seto, 2008; Geng et al., 2012). Acetylation does not seem to act on HSF2 stability by preventing the polyubiquitination of the three lysine residues, K128, K135, and K197. Indeed, only combined mutations of these lysines to 3KQ, but not to 3KR, prevent HSF2 proteasomal degradation. In addition, 3KR mutations increase HSF2 polyubiquitination, whereas 3KQ does not (Figure 6D). Previous proteome-wide quantitative analyses of the ubiquitin-modified protein have revealed that HSF2 ubiquitination occurs on multiple residues spanning over the HSF2 protein, in addition to K128, K135, and K197, including K51, K151, K210 and K420. Most of them reside in the HR-A/B domain or its vicinity, suggesting a crosstalk between acetylation and ubiquitination (Kim et al., 2011; Wagner et al., 2011; Akimov et al., 2018; www.phosphosite.org; though, note that these studies have not investigated the functional impact of these ubiquitination events on HSF2 turnover; reviewed by Gomez-Pastor et al., 2018). In addition, we showed that the acetylation of the lysine residues K128, K135, and K198 also limits the degradation of HSF2, in heat shock conditions.

We identify HDAC1 as one major HDAC involved in HSF2 deacetylation and the control of HSF2 proteasomal degradation, in basal and HS conditions, which may provide an explanation for the quick degradation of HSF2 upon HS by APC/C (Ahlskog et al., 2010). In particular, the expression of a dominant-negative HDAC1 prevents the induction of HSF2 polyubiquitination by HS. The other Class I HDACs, HDAC2 and HDAC3 might also be at play. We do not exclude that Class III HDACs, in particular SIRT1, which deacetylates HSF1, might be involved in HSF2 deacetylation, but treatment with NAM, a sirtuin inhibitor, gave inconsistent results in our hands. Finally, the interaction of HSF2 with CBP/EP300, or with HDACs is likely highly dynamics, as is its acetylation status.

We also do not exclude that other HATs might be involved in the regulation of HSF2 stability. For example, HSF1 proteasomal turnover and DNA-binding activity are regulated by EP300 or GCN5 (Westerheide et al., 2009; Zelin et al., 2012; Raychaudhuri et al., 2014). Notably, different HSF1 lysine residues are involved in these two distinct functions (reviewed by Miozzo et al., 2015). We do not

bioRxiv preprint doi: https://doi.org/10.1101/481457; this version posted December 26, 2018. The copyright holder for this preprint (which was not certified by peer review) is the author/funder. All rights reserved. No reuse allowed without permission.

know whether HSF2 acetylation might potentially regulate HSF2 activity. We did not observe overt modification in the DNA-binding activity of HSF2 3KR and 3KQ mutants, which prevent or mimic HSF2 acetylation on K128, K135, and K198, respectively (Figure S5E and F). However, the acetylation of these residues might have subtler effects, and that of others might influence HSF2 DNA-binding and function, including interaction with other partners (transcriptional co-activators or repressors), which would deserve future studies.

HSF2 destabilization and impaired heat shock response in RSTS syndrome

The accelerated turnover of the HSF2 protein in RSTS primary cells, which is counteracted by proteasome inhibition, confirms the importance of HSF2 interaction with CBP and EP300, and constitutes another indication for the role of acetylation on its stability.

RSTS is a rare genetic, autosomal dominant NDD, characterized by intellectual disability, multiple congenital anomalies, including heart and skeleton malformations, and elevated susceptibility to infections and childhood cancers (Spena et al., 2015). The two identified genes mutated of deleted in RSTS respectively represent 60% for *CBP* and 8-10% for *EP300*, of clinically diagnosed cases. The presence of one mutated allele of *CBP* or of *EP300* is sufficient to provoke this very disabling disease. This is surprising given that, not only a wild-type copy of the affected gene, but also the two wild-type alleles encoding the other protein (CBP or EP300) are present in the patients. The mutations in RTS patients are extremely diversified and can affect the protein expression, the protein-protein binding or the catalytic activity, which results in loss of specificity toward interacting partners and/or the substrates. The mutated allele *via* a rupture of this subtle equilibrium could thereby exerts a "dominant-negative" effect and and compromises compensation by the wild-type copies of the other KAT3 (Merk et al., 2018; Lopez-Atalaya et al., 2014). Accordingly, even though we neither observe reduced levels of CBP in our $RSTS_{EP300}$ hPSFs, nor of EP300 in our $RSTS_{CBP}$ hPSFs (Figure 7A-C), the presence of a catalytic inactive *CBP* or deleted KIX domain E*P300* allele is sufficient to impact HSF2 proteasomal turnover in our system (Figure 7A-C). Likewise, several lines of evidence suggest that the presence of a dominant-negative *CBP* or E*P300* allele is sufficient to impact HSF2 proteasomal turnover, in these cells. Indeed, the mutated *CBP* or of *EP300* allele, despite the presence of the other *CBP* (or, conversely, *EP300*) wild-type alleles, seems sufficient to compromise HSF2 stability and lead to its proteasomal degradation. This suggests that the presence of the dominant-negative mutated allele impairs HSF2 acetylation. In addition, VPA is unable to restore HSF2 levels in RSTS cells, likely because HSF2 is not acetylated in these cells. This reinforces the hypothesis that the integrity of EP300 and CBP function is key to the control of HSF2 levels in these cells.

HSF2 is a modulator of the HSR by fine-tuning the expression of *HSP* genes and the formation of nSBs (Östling et al., 2007; Sandqvist et al., 2009). This occurs through co-binding of HSF2 and HSF1, *via* the formation of heterotrimers, to the regulatory regions of the *HSP* genes and *SatIII* loci (Alastalo et al., 2003; Östling et al., 2007; Sandqvist et al., 2009).

First, in the RSTS context, HSF2 seems majorly deregulated (HSF1 availability being only slightly affected), and we find that the basal HSP70 and HSP90 protein levels are markedly reduced. Second, in response to HS, the magnitude of induction of HSP70 is impaired, and HSF2 thus seems to play an important role in the HSR in the PSFs cells, in line with the work of Östling et al. (2007). Moreover, we also observe that the reduction of HSF2 levels in RSTS cells affects the formation of nSBs. It is therefore possible that the HSR could be regulated at two different levels by the proteasome, providing an exquisite and sophisticated way to control cell proteostasis, *via* the stabilization of: 1) HSF1 in an EP300-dependent manner (at least in some cell systems; Raychaudhuri et al., 2014); and/or 2) HSF2, in CBP- and EP300-dependent manner (here in hPSFs). The balance between these two arms of regulation (HSF1 or HSF2-driven) could be tipped by the cell context, and potentially the HSF1/HSF2 ratio (Östling et al., 2007; Sandqvist et al., 2009).

In conclusion, equipment in chaperones is altered in RSTS cells in unstressed conditions, in a chronic manner, and in stressed conditions, this alteration might confer those cells vulnerability to proteostasis challenge.

bioRxiv preprint doi: https://doi.org/10.1101/481457; this version posted December 26, 2018. The copyright holder for this preprint (which was not certified by peer review) is the author/funder. All rights reserved. No reuse allowed without permission.

The dysregulation of the HSF pathway in RSTS, which includes marked reduction of HSF2 levels, might have several implications for this multifaceted disease. Indeed, RSTS is a neurodevelopmental disorder and HSF2, as a TF involved in neurodevelopment both in normal and stress conditions, might contribute to RSTS neurodevelopmental defects, through reduction of its availability in RSTS patient cells. Second, RSTS patients show of extreme vulnerability to airway infections, which is mainly due to deficit in mounting a response to polysaccharides (Naimi et al., 2006; Herriot et al., 2016) and because the HSF pathway is involved in response to polysaccharides, inflammatory and immune response and lung protection against stress, its deregulation could also contribute to this deficit (Xiao et al., 1999; Inouye et al., 2007; Wirth et al., 2003). Therefore, any imbalance in the delicate composition of the HSP repertoire in normal conditions and the triggering of HSF-driven stress-responses could participate to this vulnerability. Globally, the deregulation of the HSF pathway, which controls brain development, tumor initiation and progression might constitute an interesting novel reading key for this complex disease.

bioRxiv preprint doi: https://doi.org/10.1101/481457; this version posted December 26, 2018. The copyright holder for this preprint (which was not certified by peer review) is the author/funder. All rights reserved. No reuse allowed without permission.

LEGENDS OF FIGURES

Figure 1. HSF2 expression profiles, acetylation status, and interaction with EP300/CBP in brain development

(A to C) ***HSF2 and CBP/EP300 in human brain organoids exhibit similar expression profiles and territories.***

(A) Representative immunoblot of extracts from human brain organoids at day 20, 40, and 60 of *ex vivo* development (D20, D40, D60) and human ES cells (H9) at passage 17 and 23. The position of molecular weight markers is indicated (kDa). (See also Figure S1A).

(B) (a) Microscopy epifluorescence images of a D60 human organoid. (a) DAPI-staining of the complete section (image reconstruction), showing structures reminiscent of the developing cerebral cortex (arrows). The thick white rectangle indicates the magnified areas shown in (b-e). (b) phase contrast; (c) DAPI-staining; (d-f) Immunostaining for EP300 (d, f, red) and HSF2 (e, f, green), and merge (f). The thin rectangle in (f) indicates the area magnified in (C). Scale bars: in (a), 500 µm; in (b), 60 µm.

(C) Magnification of the cortical-like area indicated by the thin rectangle in (**B**; f). (a) DAPI-staining; (b-d) Immunostaining for EP300 (b) and HSF2 detection (c), and merge (d). (a1-d1) and (a2-d2) correspond to magnified regions in the zone of neurons (low DAPI density, Tuj1 positive region, see Figure S1B;e,j) and NPCs (high DAPI density, Sox2-positive region, see Figure S1B;h,i), respectively, indicated by white squares in (a, b, c, d). HSF2 and EP300 are co-expressed in some neurons (long arrows; see also Figure S1B; d,e) and NPCs (arrowheads; dense DAPI-stained regions).

(D and E) ***HSF2 interacts with EP300 and is present in an acetylated form in the developing human and mouse cortex.***

(D) Endogenous HSF2 and EP300 proteins are co-immunoprecipitated in E16.5 cortical extracts. (See also Figure S1E).

(E) Acetylation of the immunoprecipitated HSF2 protein from E13.5 cortical extracts was assessed using anti-pan-acetyl-lysine antibody (AcK; see also Figure S1E). Co-immunoprecipitation of EP300 is shown as a positive control.

(F) HSF2 is acetylated in human brain organoids. Immunoprecipitation of the HSF2 protein in D40 organoids and immunoblotting with an anti-AcK antibody. Equal loading of the inputs was assessed using actin immunoblotting.

bioRxiv preprint doi: https://doi.org/10.1101/481457; this version posted December 26, 2018. The copyright holder for this preprint (which was not certified by peer review) is the author/funder. All rights reserved. No reuse allowed without permission.

Figure 2. HSF2 is acetylated by CBP and EP300 in normal conditions.

(A) ***The ectopically expressed YFP-tagged HSF2 protein is acetylated by exogenous HA-tagged CB or EP300.*** Representative immunoblots (n = 5 independent experiments). HEK 293 cells were transfected with different combinations of YFP-tagged HSF2, HA-tagged CB, HA-tagged EP300 constructs, and mock-HA or mock GFP constructs. YFP-HSF2 was immunoprecipitated using anti-GFP-trap antibody (IP GFP-Trap) and its acetylation status was determined by Western blot (WB) analyses, using an anti-pan-acetyl-lysine antibody (AcK; upper panels). Total immunoprecipitated HSF2 was detected using an anti-GFP antibody (WB: GFP). The total amounts of HSF2 and CBP or EP300 proteins in the input samples were detected with anti-GFP and anti-HA antibodies, respectively (inputs; lower panels). Equal loading of the inputs was assessed using actin immunoblotting.

(B) The HSF2-Myc protein is not acetylated by a dominant-negative form of CBP (DNCBP-HA). HEK 293 cells were transfected as in (**A**), except that HSF2-Myc was used instead of HSF2-YFP, and immunoprecipitation was performed using anti-Myc-trap antibody (IP Myc-Trap). HSP90 was used as a loading control. Representative immunoblots (n= 2 experiments). Note that HSF2 is acetylated, whether of murine (Figure 2A) or human origin (Figure 2B).

(C) Schematic representation of the eight main acetylated lysine residues of the HSF2 protein. Purified mouse Flag-HSF2, co-expressed with HA-tagged EP300, immunoprecipitated and subjected to mass spectrometry analysis for detection of acetylated lysine residues. The three lysine residues K128, K135, K197, located in the oligomerization domain (HR-A/B), are enlightened in red and K82, located in the DBD, in blue; the other four lysine residues (K209/K210, K414/K420) are indicated in black. The DNA-binding domain (DBD, orange); the oligomerization domain (HR-A/B; green) and the domain controlling oligomerization (the leucine-zipper-containing HR-C; green); as well as the N-terminal domain (activation domain TAD; red) are illustrated. The boundaries of each domain are indicated in bold and blue. Bold and blue numbers correspond to the number of the amino acids located at boundaries of the domains of the mouse HSF2 protein, numbered from the +1 (ATG); the equivalent in the human HSF2 protein, if different, are indicated in regular and black. These four (K82, K128, K135, K197) or three lysine residues (K128, K135, K197) were mutated into glutamines (4KQ or 3KQ, respectively) or arginines (4KR or 3KR, respectively; see also Figure S2A).

(D) The mutations of three or four K residues to arginine (3KR or 4KR) or glutamine residues (3KQ or 4KQ) decrease HSF2 global acetylation levels. HEK 293 cells were co-transfected with EP300-HA and wild-type (WT) or mutated human HSF2-Myc on the indicated lysine residues. The acetylation of the corresponding immunoprecipitated HSF2 proteins using anti-Myc antibody, was analysed by WB using an anti-AcK antibody. n= 3 independent experiments. (See also Figure S2B,C).

(E) ***In vitro*** **acetylation of HSF2 peptides containing K82, K135, and K197 residues by recombinant CBP Full-HAT**. HSF2 peptide substrates were incubated in the presence of recombinant purified CBP-Full HAT and acetyl-CoA, and their acetylation analysed by reverse phase–ultra-fast liquid chromatography (RP–UFLC). (Left panel) Time course RP-UFLC analysis of HSF2 K197 acetylation by CBP Full-HAT. Aliquots of the reaction were collected at 0 (black), 1 (red) or 2 (green) hours and elution of peptides was monitored by fluorescence emission at 530 nm (excitation: 485 nm, uV: arbitrary unit of fluorescence). (Right panel) The AUC (area under the curve) of the acetylated K82, K135 and K197 peptides was quantified and converted in product concentration using a calibrated curve of various known concentrations of peptides. Note that it was not possible to investigate the acetylation of the HSF2 K128 peptide by CBP, because this peptide was repeatedly insoluble at the synthesis steps (Manufacturer's information; see also Figure S2D-F).

bioRxiv preprint doi: https://doi.org/10.1101/481457; this version posted December 26, 2018. The copyright holder for this preprint (which was not certified by peer review) is the author/funder. All rights reserved. No reuse allowed without permission.

Figure 3. HSF2 interacts with CBP and EP300 in normal conditions.

(A) ***Schematic representation of CBP protein domains***. The ability of CBP to bind a very large number of proteins is mediated by several conserved protein binding domains, including the nuclear receptor interaction domain (RID), the cysteine/histidine-rich region 1 (CH1), KIX, Bromodomain (BD), PHD, HAT, ZZ, CH3, SID (steroid receptor co-activator-1 interaction domain), and the nuclear coactivator binding domain NCBD (not illustrated here) and QP (Glutamine- and proline-rich domain; Dancy and Cole, 2015; Dyson and Wright 2016).

(B) ***Biolayer interferometry measurement of CBP binding to recombinant HSF2.***
Binding of different His-tagged domains of CBP to immobilized biotinylated recombinant HSF2 on streptavidin sensor tips (recHSF2): the catalytic full domain "Full-HAT", or one of the following subdomains: PHD, HAT, RING, or Bromodomain (BD). HSP70 was used as a positive control for binding to HSF2 (Tang et al., 2016; see Figure S3A for determination of the Kd).

(C) ***The ectopically expressed YFP-tagged HSF2 protein interacts with exogenous HA-tagged CBP.*** HEK 293 cells were transfected with combinations HSF2-YFP and CBP-HA, or mock-HA (or mock-GFP) constructs. (Upper panels) HSF2-YFP was immunoprecipitated using anti-GFP-trap antibody (IP GFP-Trap) and co-immunoprecipitated CBP protein was detected by using anti-HA antibody. The immunoprecipitated HSF2 was detected using an anti-GFP antibody. The total amounts of exogenous HSF2 and CBP proteins in the input samples were detected with anti-GFP and anti-HA antibodies, respectively (inputs; lower panels). Equal loading of the inputs was assessed using actin immunoblotting. Representative immunoblots (n= 3 experiments).

(D) ***The ectopically expressed YFP-HSF2 protein interacts with exogenous EP300.*** As in (**A**) except that HEK 293 cells were transfected with an EP300-HA construct. Representative immunoblots (n= 3 experiments).

(E) ***Principle of the fluorescent-3-hybrid (F3H) assay.***

(F) ***F3H assay for the visualization of interaction between HSF2-YFP and exogenous CBP-HA or endogenous CBP*** (upper and lower panels, respectively). (Left) Confocal sections of BHK cells carrying a stably integrated Lac-operator array that were triple transfected with *LacI* fused to the GFP-binder, HSF2-YFP, and CBP-HA constructs. Exogenous and endogenous CBP was detected using an anti-HA or an anti-CBP antibody, respectively (red signal). Chromatin was counterstained using DAPI. All the experiments involving negative controls are shown in Figure S3C,D. White arrows point out localization of HSF2-YFP and CBP-HA at the *LacO* spot. Scale bar, 10 µm. (Right) Graphs represent the quantification of the intensity of the two fluorescence signals, visualizing the co-localization of HSF2-YFP and CBP-HA signals to the *LacO* array (x/µ; y/µ; z, signal intensity in arbitrary units). "Number of + cells": quantification of the percentage of cells showing co-recruitment of YFP-HSF2 and CBP-HA or endogenous CBP, in the *LacO* array. Representative images, n = 3 independent experiments for CBP-HA and n= 3 for endogenous CBP.

(G) ***F3H assay for the visualization of interaction between HSF2-YFP and exogenous EP300-HA.*** As in Figure 3E, except that exogenous EP300-HA was detected using an anti-HA antibody (red signal). All the negative controls are shown in Figure S3E. "Number of + cells": quantification of the percentage of cells showing co-recruitment of HSF2 and EP300 in the Lac0 array. Representative images, n = 4 independent experiments.

bioRxiv preprint doi: https://doi.org/10.1101/481457; this version posted December 26, 2018. The copyright holder for this preprint (which was not certified by peer review) is the author/funder. All rights reserved. No reuse allowed without permission.

Figure 4. Modelling of CBP and HSF2 interaction.

(A) ***Schematic representation of the KIX-binding motifs located in the HSF2 HR-A/B region*****.**
Conserved KIX-binding motif sequences ("ΦXXΦΦ") are indicated (blue rectangle). The positions of the very conserved, major acetylated lysine residues are highlighted: K82 located in the DBD, K128, K135, and K197 located in the HR-A/B domain (in red), and K209/K210, located downstream the HR-A/B (in black).

(B) In vitro ***interaction between the KIX-GST domain of CBP and the SNAP-HSF2 protein***. The recombinant KIX-GST and SNAP-HSF2 proteins were produced in bacteria and reticulocyte lysates, respectively, and subjected to an *in vitro* co-immunoprecipitation using an anti-GST antibody.

(C) In silico ***model structure of CBP KIX domain and HSF2 HR-A/B interaction.***
CBP KIX domain (in green): Representation of the KIX domain of CBP, a triple helical globular domain. The c-Myb surface of the KIX-domain is indicated in red. HSF2 HR-A/B domains (in blue): Representation of the HSF2 HR-A/B domains of the HSF2 trimer, as a triple-coiled coil. The KIX recognition motifs of HSF2 are indicated in red.

(D) ***Magnification of the*** **in silico** ***representation illustrated in (C)*** showing the positioning of the tyrosine residue Y650 in the c-Myb surface of the CBP KIX domain and the contact of this Y650 to the KIX recognition motifs located in the HSF2 HR-A/B domain.

(E) In silico ***representation of the positioning of 4 residues located within the HSF2 KIX recognition motifs, and of Y650 within the CBP KIX domain that have been analyzed after*** **in silico** ***mutation*** (see (D-F) and Figure S4F).

(F) In silico (upper panel) ***and*** **in vitro** (lower panel) **Y650A mutation in the CBP KIX domain disrupt interaction between the HSF2 KIX motif and the CBP KIX domain** (see also Figure S4F,b).

bioRxiv preprint doi: https://doi.org/10.1101/481457; this version posted December 26, 2018. The copyright holder for this preprint (which was not certified by peer review) is the author/funder. All rights reserved. No reuse allowed without permission.

Figure 5. Impact of preventing or mimicking acetylation of lysine residues K218, K135, and K197 on HSF2 protein stability.

(A) ***Inhibiting CBP/EP300 decreases HSF2 protein levels, a process counteracted by proteasome inhibition.*** (Upper panels) Representative immunoblot of HSF2 and CBP levels upon treatment of N2A cells with the CBP/EP300 inhibitor C646 (40µM for 4 h) and/or with the proteasome inhibitor MG132 (20 µM for 6h). n = 4 independent experiments. Standard deviation is indicated. * $p<0.05$. (Lower panels) decreased acetylation levels of lysine residue K18 of histone H3 (H3K18Ac) assessed C646 efficiency in inhibiting CBP/EP300 activity. Cognate, non-inducible, HSC70 protein: loading control.

(B) ***Schematic representation of the principle of SNAP-TAG-based pulse-chase experiments***. Cells expressing SNAP-tagged HSF2 are incubated in the presence of a fluorescent substrate, which, at a given time (t_0), covalently labels the pool of SNAP-tagged HSF2 molecules present in the cell. The addition of a non-fluorescent, blocking substrate prevents further labelling of the newly synthesized HSF2 molecules. It therefore allows the measurement of the decay in the fluorescent signal corresponding to SNAP-tagged-HSF2 molecules covalently bound by the fluorescent substrate, thereby allowing an estimation of the decay in HSF2 protein levels.

(C) ***Combined mutations of lysine residues K128, K135, and K197 mimicking HSF2 acetylation (3KQ) slow down the decay of HSF2 protein levels, compared with HSF2 WT, in contrast to mutations preventing acetylation (3KR)***. Representative gel analysis of decay in HSF2 protein levels, carrying 3KR or 3KQ mutations, and labelled by the fluorescent SNAP-substrate, in CRISPR-Cas9 *Hsf2*KO U2OS cells. SNAP-H3.3 is used as a loading control.

(D) ***Quantification of the fluorescent signal*** corresponding to SNAP-HSF2 WT (blue), 3KQ (red), or 3KR (green), as a measure of of SNAP-HSF2 protein decay. n = 7-10 independent experiments. Standard deviation. t45'-t3h * $p<0.05$; t5h** $p<0.01$.

(E) ***The decrease in SNAP-HSF2 WT and 3KR protein levels depends on proteasome activity***. As in (C), but cells were pre-treated with 10 or 20 µM MG132 for 6 h. n = 2 independent experiments.

bioRxiv preprint doi: https://doi.org/10.1101/481457; this version posted December 26, 2018. The copyright holder for this preprint (which was not certified by peer review) is the author/funder. All rights reserved. No reuse allowed without permission.

Figure 6. Impact of HDAC1 on HSF2 levels in normal and stress conditions.

(A) ***Identification of HDAC1 as a HSF2 protein partner in TAP-TAG/MS analysis in HeLa-S3 cells***. After sequential immunoprecipitation of nuclear extracts of HeLa-S3 expressing CTAP-HSF2α and CTAP-HSF2β, using two tags (G-protein and Streptavidin-binding peptide; see Figure S6A), eluates were analyzed by MS. The number of unique peptides from each identified protein and their UniProt Knowledgebase (UniProtKB) codes are indicated. Three different MS analyses.

(B) ***Interaction between ectopically expressed HDAC1-GFP and HSF2-Flag in F3H assays***. As in Figure 3F, except that BHK cells were triple transfected with *LacI* fused to the GFP-binder, HDAC1-GFP, and HSF2-Flag constructs. Chromatin was counterstained using DAPI. All the negative controls are shown in Figure S6E. n = 3 independent experiments.

(C) ***The ectopically expressed exogenous HDAC1 interacts with HSF2.*** (Upper panel). GFP-Trap co-immunoprecipitation of HDAC1-GFP and HSF2-Myc in transfected HEK 293 cell extracts. (Middle and lower panels) Immunoblot showing total HDAC1 (WB GFP) or HSF2 levels (WB Myc) in inputs, respectively. n=2 independent experiments.

(D) ***The HSF2 3KR mutation, which prevents HSF2 acetylation, favours HSF2 polyubiquitination, whereas 3KQ, mimicking HSF2 acetylation, does not.*** HEK 293 cells were co-transfected with Myc-tagged HSF2 wild-type or mutated on three lysines K128, K135, and K197 (3KR), and treated or not with the proteasome inhibitor, MG132 (MG; 20µM for 6 h). HSF2 was immunoprecipitated using anti-Myc antibody and its polyubiquitination status was analysed by WB, using an anti-ubiquitin antibody. The protein amounts in the input samples were detected with antibodies against HSF2 and HSC70. (n=3 independent experiments, at least)

(E) ***Overexpression of HDAC1 markedly reduces the acetylation of HSF2 by CBP.*** HEK 293 cells were transfected by the following constructs: CBP-HA and HSF2-Flag, and HDAC1-Flag, HDAC2-Myc, or HDAC3-Myc and the acetylation status of the HSF2-Flag protein was checked by using an anti-AcK antibody. n=5 independent experiments. Standard deviation. **, $p < 0.05$; *** $p < 0.001$. Actin was used as a loading control.

(F) ***The stability of HSF2 3KQ is increased upon HS, compared with HSF2 WT or HSF2 3KR***. (Upper panel) Representative gel analysis of HSF2 protein decay in a SNAP-TAG pulse-chase experiment. As in Figure 5C, except that cells were submitted to HS at 42°C for the indicated times. (Lower panel) Quantification on the signal intensity. n=5 independent experiments. Standard deviation. * $p<0.01$; ** $p<0.001$. SNAP-H3.3 was used as a loading control.

(G) ***Class I HDAC inhibitor VPA prevents the decrease in endogenous HSF2 protein levels induced by HS***. N2A cells were pretreated or not with 1 mM valproic acic (VPA) for 3 h and subjected to HS 42°C for 1 h. (Upper panel) Representative immunoblot. (Lower panel) Quantification on the signal intensity normalized to actin levels (n=4 independent experiments). *** $p<0.001$.

(H) ***Expression of dominant-negative HDAC1 prevents the accumulation of polyubiquinated HSF2 upon HS***.HEK 293 cells were cotransfected with HSF2-Myc, EP300-HA, and Flag-HDAC1 or dnHDAC1, and subjected or not to HS 42°C (30 min). Representative immunoblot of polyubiquinated HSF2 levels after Myc-HSF2 immunoprecipitation. (n=3 independent experiments, at least).

bioRxiv preprint doi: https://doi.org/10.1101/481457; this version posted December 26, 2018. The copyright holder for this preprint (which was not certified by peer review) is the author/funder. All rights reserved. No reuse allowed without permission.

Figure 7. Altered HSF2 protein levels and dysregulated stress response in cells from RSTS patients.

(A) ***HSF2 levels are reduced in RSTS$_{CBP}$ hPSFs (patient P1), but restored in the presence of the proteasome inhibitor MG132***. See Figure S7A for the description of the patient's mutations. (Left panel) Representative immunoblot. (Right panel) Comparison of the H3K27 acetylation status in RSTS and HD. In contrast, the HDAC inhibitor VPA does not restores HSF2 levels (Figure S7B, and see Figure S7C for the assessment of VPA efficiency). n=3 experiments.

(B) ***HSF2 levels are reduced in RSTS$_{EP300}$ hPSFs (patient P2), but restored in the presence of the proteasome inhibitor MG132.*** (Left panel) Cells were treated with 20 µM MG132 (6 h) or 1 mM of the HDAC inhibitor VPA (3 h) and subjected to immunoblot analysis. (Right panel) Comparison of the H3K27 acetylation status in RSTS and HD. n = 3 experiments.

(C) ***HSF2 staining is reduced in RSTS$_{EP300}$ hPSFs.*** Representative immunofluorescence experiments. n = 3 experiments.

(D) ***Reduced HSP basal levels and induction by heat shock in RSTS$_{EP300}$ hPSFs.*** (Left panel) Representative immunoblot. CTR, control conditions; HS, heat shock conditions (1 h at 42°C); Rec, recovery for 2 h. n = 3 experiments. (Right panel) quantification of the HSF2 signal in immunoblots.

(F) ***Altered formation of nSBs by HS in RSTS$_{EP300}$ hPSFs.*** (Left panels) Representative pictures of cells in control (CTR) or heat shock conditions (HS; arrowheads point to nuclear stress bodies (nSBs)). The white rectangles point out two examples of the magnified cells, positive for nSBs. (Right panel) Quantification of the percentage of cells positive for nSBs. n = 3 experiments. Number of cells counted: 100 -150. Scale bar: 10 µm. (Lower panel) Quantification of the percentage of fibroblasts positive for nSBs, from 100 – 150 cells in n = 3 different experiments. Standard deviation. RSTS *hPSFs* were compared to HD *hPSFs*. *** $p < 0.001$.

bioRxiv preprint doi: https://doi.org/10.1101/481457; this version posted December 26, 2018. The copyright holder for this preprint (which was not certified by peer review) is the author/funder. All rights reserved. No reuse allowed without permission.

LEGENDS OF SUPPLEMENTAL FIGURES

Figure S1. (related to Figure 1)

(A) ***HSF2, EP300, and CBP (CREBBP) mRNAs are expressed along the differentiation process of human brain organoids.*** RNA-Seq data in two independent sets of D20 embryoid bodies (EB_20d_A and _B), D40 (ORG_40d_A and _B), and D60 (ORG_60d_A and _B) organoids. Upper panel: The amount of mRNAs is expressed as RPKM (reads/kb/million mapped reads). Lower panel: Graph corresponding to the RNA-Seq data.

(B) ***HSF2 is expressed in areas containing NPCs and neurons.*** Upper and lower panels (a) whole view of a section of two different human organoids. The white rectangle indicates the magnified areas in (b-e) in the two panels. (b) phase contrasts. (c) DAPI staining.
(Upper panels) HSF2 is expressed (d; red) in DAPI-dense area (c) and in the area of Tuj1-positive neurons (e; green). Scale bar (a): 500 µm. As indicated by thin rectangles in (c, d, and e), (c1, d1, and e1) and (c2, d2, and e2) the magnified areas in the zones of low DAPI density-high Tuj1 signal and high DAPI density-low Tuj1 signal, correspond to neurons (arrows) and NPCs (arrowhead), respectively, as shown in the lower panels.
(Lower panels) DAPI-dense areas (h) correspond to Sox2-positive (i; red) and Tuj1-negative cells (j), that is, to NPCs. Tuj1-positive cells (j; neurons; green). Scale bars: (a) 500 µm, (b-e) 50 µm; lower panels, (a,f) 300 µm, (b-e, g-j) 50 µm.

(C) ***CBP is expressed in areas containing NPCs and neurons***. CBP staining corresponds to cells of dense DAPI staining (NPCs) and also some Tuj1 positive cells (green; neurons). Scale bar: 50 µm.

(D) ***HSF2, CBP, EP300 are expressed at all stages of mouse cortical development***. The expression profile of HSF2 is in line with our previous data (Rallu et al., 1997; Kallio et al., 2002; Chang et al., 2006; El Fatimy et al. 2014). WB analysis at from E11 to E17 of gestation.

(E) ***HSF2 interacts with EP300 and is present in an acetylated form in the E10 mouse cortex.*** Upper panels: (Left panel) Co-immunoprecipitation of endogenous EP300, and CBP proteins using anti-HSF2 antibody, and (Right panels) acetylation of the immunoprecipitated HSF2 protein from E10 cortical extracts (the blot was incubated with anti-pan-AcK antibody (WB:AcK) and then re-incubated with anti-HSF2 antibody (WB:HSF2). Lower panels: inputs. *, HSF2 forms of higher molecular weights, possibly corresponding to additional post-translational modifications, like sumoylation.

(F) Endogenous HSF2 is acetylated in the human neural precursor cell line SHSY-5Y. Endogenous HSF2 was immunoprecipitated from SHSY-5Y cells pre-treated with MG132 (20 µM for 6 hours) to increase HSF2 protein levels and optimize its detection (Mathew et al., 2008; Ahlskog et al., 2010), and its acetylation status was explored using anti-Pan-AcK antibody, as in (**E**).

bioRxiv preprint doi: https://doi.org/10.1101/481457; this version posted December 26, 2018. The copyright holder for this preprint (which was not certified by peer review) is the author/funder. All rights reserved. No reuse allowed without permission.

Figure S2. HSF2 is acetylated by CBP and EP300 in normal conditions. (related to Figure 2).

(A) ***Positioning of the acetylated peptides identified in mass spectrometry analysis in the mHSF2β protein***. Each peptide is represented as a line and numbered in red. The color code corresponds to the different HSF2 domains, as in Figure 2C. The peptides and their sequences are also listed in Table S1.

(B) ***Comparative impact of the mutations of single residues*** **(K82, K128, K135, and K197), and of the doublet K209/K210 on HSF2 acetylation by EP300**. HEK 293 cells were co-transfected with EP300-HA and wild-type HSF2-Myc (WT) or a mutated HSF2 on the indicated lysine residues. HSF2 was immunoprecipitated using an anti-Myc antibody and its acetylation was detected using a pan-acetyl-lysine (AcK) antibody.

(C) ***Impact of the combined mutations of 3 lysines (K128, K135, and K197) or 4 lysines*** **K82, K218, K135, and K197)** ***into glutamines (3KQ or 4KQ) or arginines (3KR or 4KR) on the acetylation levels of HSF2.*** HEK 293 cells were co-transfected with CBP-HA and the different HSF2-Myc constructs (wild-type (WT) or indicated mutants).

(D) ***Kinetics of*** **in vitro** ***acetylation of HSF2 peptides containing K82 (left) and K135 residues (right).*** RP–UFLC experiments. As in Figure 2E.

(E) ***Control experiments for the determination of the elution profiles*** of the K82 and acetylated K82 (AcK82), K135 and AcK135, and K197 and AcK197 peptides, using non-acetylated and synthetically acetylated commercial peptides. Separation was monitored by RP-UFLC.

(F) ***Control experiments for Acetyl-CoA-dependent acetylation of HSF2 K82, K135 and K197 peptide in the presence of CBP-Full HAT.*** HSF2 peptide substrates were incubated in the presence of recombinant purified CBP-Full HAT and with or without acetyl-CoA for 20 minutes. Acetylated products were then analysed by RP-UFLC.

bioRxiv preprint doi: https://doi.org/10.1101/481457; this version posted December 26, 2018. The copyright holder for this preprint (which was not certified by peer review) is the author/funder. All rights reserved. No reuse allowed without permission.

Figure S3. HSF2 interacts with CBP and EP300 in normal conditions. (related to Figure 3).

(A) ***Determination of the Kd of CBP Full-HAT domain affinity to HSF2.*** Biolayer interferometry to determine association and dissociation curves of CBP Full-HAT domain (concentration range from 12.5 µM to 400 nM) with biotinylated HSF2 immobilized on streptavidin sensor tips (blue curves). As a positive control the binding profile of HSP70 (100 mM) is plotted (red curve).

(B) ***Interaction between endogenous HSF2 and CBP/EP300 proteins in neural cells.***
N2A cells were treated or not (-) for 3 hours with VPA (1mM) and endogenous HSF2 was immunoprecipitated from neural precursor cells N2A. HSF2 and co-precipitated CBP (upper panels) or EP300 proteins (lower panels) were detected by WB. The total amounts of HSF2 and CBP proteins in the input samples were detected by WB. Actin is used as a loading control. *: IgG heavy chain. Representative immunoblots (n= 3 experiments).

(C) ***F3H control experiments for the visualization of interaction between HSF2-YFP and exogenous CBP-HA***. As in Figure 3F (upper panels). Scale bar: 10 µm.

(D) ***F3H control experiments for the visualization of interaction between HSF2-YFP and endogenous CBP***. As in Figure 3F (lower panels). Scale bar: 10 µm.

(E) ***F3H control experiments for the visualization of interaction between HSF2-YFP and exogenous EP300-HA.*** As in Figure 3G. Scale bar: 10 µm.

bioRxiv preprint doi: https://doi.org/10.1101/481457; this version posted December 26, 2018. The copyright holder for this preprint (which was not certified by peer review) is the author/funder. All rights reserved. No reuse allowed without permission.

Figure S4. Identification of the HSF2 domains that interact with CBP (related to Figure 4).

(A) ***Qualitative summary of the impact of the deletion of different functional domains in the wild type (WT) Flagged-HSF2 on its acetylation status and interaction with CBP-HA***, corresponding to experimental data shown in (C-D). (+++) strong; (+) moderate; (+/-) low acetylation or interaction; (ND) non detectable: in that case, the Flag tag is not recognized by the antibody, likely because it is masked by the aberrant conformation of the truncated HSF2 protein; (-*) not observed (the interaction might be very labile in the absence of the TAD domain, a typical docking site for CBP in many TFs.

(B and C) ***Determination of the HSF2 domains necessary for HSF2 acetylation by CBP-HA***

HEK 293 cells were transfected with CBP-HA and the WT HSF2-Flag or its different deleted forms.

(B) Representative immunoblot of HSF2 acetylation by CBP-HA (upper panel), comparing WT Flag-HSF2 with the HSF2 deleted forms described in (A). Second panel from the top: The HSF2 acetylation status was determined by WB using an anti-Pan-acetyl-lysine antibody (WB: AcK) and the membrane was re-incubated with anti-Flag antibody (WB:Flag) to verify the equivalent expression levels of the different HSF2 constructs.

(C) Upper panel: immunoprecipitated WT or deleted HSF2-Flag was checked for acetylation acetylation as in (B). Lower panel (negative control): WT HSF2-Flag is not acetylated in the absence of CBP-HA. Asterisks point to the acetylated forms of the WT and deleted HSF2 forms.

(D) ***Determination of HSF2 domains involved in the interaction with CBP.***

Co-immunoprecipitation of CBP-HA with wild-type or deleted HSF2-Flag was checked using anti-HA antibody (upper panel) and anti-Flag (lower panel) antibody to verify the comparable expression level of HSF2 constructs.

(E) (Upper panel) ***Ramachandran plot*** ((Discovery studio) showing the good quality of the triple coiled-coil model structure of the HR-A/B determined based on the sequence similarity of the following proteins (see Figure 4C). (Lower panel) A sequence alignment of HR-A/B (from aa. 121 to 201) between human HSF2 HR-A/B, lipoprotein Lpp56 of E. coli, yeast transcriptional factor GCN4 (mutated on some residues to generate stabilized heptad repeats) and murine PTRF and human ATF2 transcription factors (Shu *et al.,* 1999, 2000; Sandqvist *et al.,* 2009). The alignment was developed, using *Discovery Studio* and *Clustal W multiple sequence alignment program*). Colors (using *Clustal X* Colour Scheme): hydrophilic (blue); positively charged (red); negatively charged (magenta); cysteines (pink); glycines (orange); prolines (yellow); aromatic (cyan); unconserved (white).

(F) In silico ***analysis of the single mutations Y650A in the CBP KIX domain, F181, V183, K177, and Q180A in the HSF2 KIX recognition motif embedded in the HRA/B domain***. The mutations Y650A, K177A and Q180A hamper the interaction between the HR-A/B domain and KIX domain while F181A and V183A have no effect. Relative to Figure 4E.

bioRxiv preprint doi: https://doi.org/10.1101/481457; this version posted December 26, 2018. The copyright holder for this preprint (which was not certified by peer review) is the author/funder. All rights reserved. No reuse allowed without permission.

Figure S5. (related to Figure 5).

(A) ***Dose dependent-decrease in HSF2 protein levels upon treatment with C646 CBP/EP300 inhibitor***.

Representative immunoblot of HSF2 protein levels in N2A cells treated 20 or 40 µM of the HAT inhibitor C646 for 4 hours or with the vehicle (DMSO, CTL). Relative to Figure 5A.

(B) ***Sequence of the HSF2 alleles mutated in U2OS cells using the CRISPR/Cas9 KO strategy and corresponding protein products***.

(C) ***Representative immunoblot analysis of HSF2 content in the CRISPR/Cas9 Hsf2KO cells***. U2OS parental and SHSY-5Y cell extracts were loading as positive controls for the detection of HSF2. Actin, loading control.

(D) ***Myc-tagged HSF2WT, HSF2 3KQ, HSF2 3KR, and HSF2 4KR are ectopically expressed at similar levels in 2KO cells***. Representative immunoblot analysis of transient transfection experiments with the corresponding constructs. Actin, loading control.

(E) ***Ectopically expressed Myc-tagged HSF2WT, and mutant HSF2 3KQ, HSF2 3KR, and HSF2 4KR exhibit HSF2 DNA-binding activity* ex vivo**. Gel-shift analysis of HSF1 and HSF2 DNA-binding activity in *2*KO cells, expressing Myc-tagged HSF2WT, HSF2 3KQ, HSF2 3KR, or HSF2 4KR, (or Myc (mock) as a negative control). The presence of HSF1 and/or HSF2 in the HSF-HSE complex was analyzed by supershifting (arrowhead) with anti-HSF1 (α1; black arrowhead) or anti-HSF2 (α2; white arrowhead), or anti-Myc antibodies (α-Myc; blue arrowhead). Note that non-transfected *2*KO U2OS cells (-) were devoid of any HSF DNA-binding activity (absence of HSF-HSE complex). N2A cells were loaded as positive controls for anti-HSF2 antibodies. Notably, *2*KO cells expressing HSF2WT, HSF2 3KQ, HSF2 3KR, and HSF2 4KR proteins allow the formation of a HSE-HSF complex, which is mainly supershifted by anti-HSF2 (but mostly not by anti-HSF1), whereas, as expected, mocked transfected *2*KO cells are devoid of HSF2 activity. HSF-HSE: HSF-HSE complexes. CHBA: constitutive HSE-binding activity, which is not carried by HSFs and is very variable from one sample or condition to another (Mosser et al., 1988; Abravaya et al., 1991); NS: non-specific DNA-protein complex; free: unbound double-stranded HSE oligonucleotide.

(F) ***Myc-HSF2WT, HSF2 3KQ, or HSF2 3KR proteins localize into nuclear-stress bodies upon HS.*** Immunofluorescence analysis of the ability of the WT or mutated HSF2 to localize to nSBs when ectopically expressed in U2OS cells, in response to a 1h HS at 42°C, using anti-Myc antibodies. Scale bar: 20 µm.

bioRxiv preprint doi: https://doi.org/10.1101/481457; this version posted December 26, 2018. The copyright holder for this preprint (which was not certified by peer review) is the author/funder. All rights reserved. No reuse allowed without permission.

Figure S6. Impact of HDAC1/2 on HSF2 levels in normal and stress conditions. (related to Figure 6).

(A) ***Schematic representation of the two-step TAP-TAG approach for identification of HSF2 partners in the nucleus of HeLa-S3 cells*** (Bürckstümmer et al., 2006) transfected with PCEMM-CTAP-HSF2α or PCEMM-CTAP-HSF2β, using the G-protein (in yellow) and streptavidin binding peptide (SBP in orange), as dual affinity tags (GS-TAP), sequentially. Relative to Figure 6A.

(B) ***Analysis of whole cell (Tot), cytosolic (Cyto), and nuclear (Nuc) extracts*** from the HeLa-S3-CTAP-empty, HeLa-S3-CTAP-HSF2α and HeLa-S3-CTAP-HSF2β cell populations. Enrichment in histones in nuclear fractions by Coomassie blue was verified in a first step (data not shown). Relative to Figure 6A.

(C) ***Silver staining of SDS-PAGE analyses of final double-TAP-TAG eluates*** from HeLa-S3-CTAP-empty, HeLa-S3-CTAP-HSF2α and HeLa-S3-CTAP-HSF2β nuclear extracts. Relative to Figure 6A.

(D) ***Identification of HDAC1 and 2 as HSF2 protein partners by MS in the E17 mouse brain cortex***. Upper panel: colloidal blue staining of the gel where the samples were run prior to MS analysis, after HSF2 immunoprecipitation from the E17 fetal telencephalon. The rectangles delimit the gel bands that were cut and subjected to MS. The asterisk indicates the gel band from which HDAC1 and HDAC2 peptides were identified (see lower panel). Lower panel: number of unique peptides from each identified protein and their UniProt Knowledgebase (UniProtKB) codes are indicated.

(E) ***F3H control experiments for the visualization of the interaction between HSF2-Flag and exogenous HDAC1-GFP***. As in Figure 6B. Scale bar: 10 µm.

(F) ***HDAC8 does not affect HSF2 acetylation levels, in contrast to HDAC1.*** Relative to Figure 6E. Standard deviation, * p<0,05.

(G) ***Endogenous HSF2 levels are decreased upon HS in N2A cells***. Representative immunoblot and quantification of n= 3 experiments. Standard deviation, * p<0,05.

(H) ***Control experiment for the efficiency of HDAC inhibitor VPA in N2A cells***. Representative immunoblot for H3K27 acetylation (AcH3K27). Relative to Figure 6G.

bioRxiv preprint doi: https://doi.org/10.1101/481457; this version posted December 26, 2018. The copyright holder for this preprint (which was not certified by peer review) is the author/funder. All rights reserved. No reuse allowed without permission.

Figure S7. Altered HSF2 protein levels and dysregulation of the stress response in RSTS. (related to Figure 7).

(A) ***Description of the mutations or deletions present in RSTS patients.*** The scheme of the genomic organization of the genes are taken from https ://www.ncbi.nlm.nih.gov/nuccore/NM_001429.3

RSTS hPSFs were isolated from two patients (P1 and P2):

Patient P1- hPSF RSTS$_{EP300}$: Deletion of at least 10 kb (chr22:41533381.41543435) and to the maximum of 11 kb (chr22:41532396.41543758) confirmed by quantitative multiplex fluorescent (QMF)-PCR. This mutation leads to a truncated protein, with deletion of a binding site, the KIX domain, which is essential for the interaction between HSF2 and EP300/CBP proteins. We show that hPSF exhibit a decreased level in H3K27 acetylation compared to HD as expected in this cell model (Jin, PMID: 21131905).

Patient P2- hPSF RSTS$_{CBP}$: Mutation pLys1139X (exon 18) located in the catalytic CBP HAT domain, needed for its acetyltransferase activity. This mutation did not affect CBP or EP300 levels and a marked impact on H3K27 acetylation was observed (Figure 7A).

Lymphoblastoid cells were derived from three patients (P3-P5):

Patient P3- LB RSTS$_{EP300}$: Mutation pTrp1649X (Exon 30) in *EP300 gene* which gives rise to a stop codon in the HAT domain leading to a C-terminal deletion. This mutation leads to >50% decrease of EP300 protein level with a predicted altered activity (MutPred2).

Patient P4- LB RSTS$_{CBP}$: Deletion in 5' (2 first exons) in *CREBBP gene*. This mutation leads to a truncated protein and decrease in CBP protein levels.

Patient P5- LB RSTS$_{CBP}$: Mutation p.Arg1498* (exon 27) located in the catalytic CBP HAT domain with formation of a stop codon leading to a C-terminal deletion. This mutation leads to a clear decrease of CBP protein level.

(B) ***Assessment of the efficiency of the VPA treatment in RSTS$_{EP300}$ hPSFs (patient P2)***, in increasing in H3K27 acetylation. Related to Figure 7B.

(C) ***VPA does not increase HSF2 levels in RSTS$_{CBP}$ (patient P1) hPSFs***, in contrast, to what happens in HD cells. Relative to Figure 7A.

(D) ***HD and in RSTS$_{EP300}$ hPSFs (patient P2) contain similar levels of HDAC1***.

(E) ***Formation of nSBS, with HSF1 and EP300 expression in HD and RSTS$_{EP300}$ hPSFs, upon HS.*** Representative immunofluorescence experiment, in control (CTR) or HS conditions (1 hour at 42°C). Scale bar: 20 µm. Relative to Figure 7E.

(F) ***Altered formation of nSBs by HS in RSTS$_{EP300}$ or RSTS$_{CBP}$ LBs.*** (Left panel) Representative pictures of cells in HS conditions (1 hour at 43°C). (Right panel) Quantification of the percentage of cells positive for nSBs, from 100 – 150 cells in n = 3 different experiments. Standard deviation. RSTS LBs were compared to HD LBs. *, $P < 0.05$; **, $p < 0.01$. For P3 (RSTS$_{EP300}$), p = 0.00125903; for P4 (RSTS$_{CBP}$), 0.01446243; for P5 (RSTS$_{CBP}$), p = 0.01123926.

bioRxiv preprint doi: https://doi.org/10.1101/481457; this version posted December 26, 2018. The copyright holder for this preprint (which was not certified by peer review) is the author/funder. All rights reserved. No reuse allowed without permission.

References

Ahlskog JK, Björk JK, Elsing AN, Aspelin C, Kallio M, Roos-Mattjus P, Sistonen L. Anaphase-promoting complex/cyclosome participates in the acute response to protein-damaging stress. Mol Cell Biol. 2010 Dec;30(24):5608-20. doi: 10.1128/MCB.01506-09. PMID: 20937767

Alarcón JM, Malleret G, Touzani K, Vronskaya S, Ishii S, Kandel ER, Barco A. Chromatin acetylation, memory, and LTP are impaired in CBP+/- mice: a model for the cognitive deficit in Rubinstein-Taybi syndrome and its amelioration. Neuron. 2004 Jun 24;42(6):947-59. PMID: 15207239

Alastalo TP, Hellesuo M, Sandqvist A, Hietakangas V, Kallio M, Sistonen L. Formation of nuclear stress granules involves HSF2 and coincides with the nucleolar localization of Hsp70. J Cell Sci. 2003 Sep 1;116(Pt 17):3557-70. Epub 2003 Jul 15. PMID: 12865437

Aasland R, Gibson TJ, Stewart AF. The PHD finger: implications for chromatin-mediated transcriptional regulation.Trends Biochem Sci. 1995 Feb;20(2):56-9. PMID: 7701562

Anckar J, Sistonen L. Regulation of HSF1 function in the heat stress response: implications in aging and disease. Annu Rev Biochem. 2011;80:1089-115. doi: 10.1146/annurev-biochem-060809-095203. Review. PMID: 21417720

Akimov V, Barrio-Hernandez I, Hansen SVF, Hallenborg P, Pedersen AK, Bekker-Jensen DB, Puglia M, Christensen SDK, Vanselow JT, Nielsen MM, Kratchmarova I, Kelstrup CD, Olsen JV, Blagoev B. UbiSite approach for comprehensive mapping of lysine and N-terminal ubiquitination sites. Nat Struct Mol Biol. 2018 Jul;25(7):631-640. doi: 10.1038/s41594-018-0084-y. Epub 2018 Jul 2. PMID: 29967540

Babu A, Kamaraj M, Basu M, Mukherjee D, Kapoor S, Ranjan S, Swamy MM, Kaypee S, Scaria V, Kundu TK, Sachidanandan C. Chemical and genetic rescue of an ep300 knockdown model for Rubinstein Taybi Syndrome in zebrafish. Biochim Biophys Acta. 2018 Apr;1864(4 Pt A):1203-1215. doi: 10.1016/j.bbadis.2018.01.029. Epub 2018 Jan 31. PMID: 29409755

Bhattacherjee V, Horn KH, Singh S, Webb CL, Pisano MM, Greene RM. CBP/p300 and associated transcriptional co-activators exhibit distinct expression patterns during murine craniofacial and neural tube development. Int J Dev Biol. 2009;53(7):1097-104. doi: 10.1387/ijdb.072489vb. PMID: 1959812

Björk JK, Åkerfelt M, Joutsen J, Puustinen MC, Cheng F, Sistonen L, Nees M. Heat-shock factor 2 is a suppressor of prostate cancer invasion. Oncogene. 2016 Apr 7;35(14):1770-84. doi: 10.1038/onc.2015.241. PMID: 26119944

Björk JK, Sandqvist A, Elsing AN, Kotaja N, Sistonen L. miR-18, a member of Oncomir-1, targets heat shock transcription factor 2 in spermatogenesis. Development. 2010 Oct;137(19):3177-84. doi: 10.1242/dev.050955. Epub 2010 Aug 19. PMID: 20724452

Bodor DL, Rodríguez MG, Moreno N, Jansen LE. Analysis of protein turnover by quantitative SNAP-based pulse-chase imaging. Curr Protoc Cell Biol. 2012. Jun; Chapter 8:Unit 8.8. doi: 10.1002/0471143030.cb0808s55. PMID: 23129118

Bordoli L, Hüsser S, Lüthi U, Netsch M, Osmani H, Eckner R. Functional analysis of the p300 acetyltransferase domain: the PHD finger of p300 but not of CBP is dispensable for enzymatic activity. Nucleic Acids Res. 2001 Nov 1;29(21):4462-71. PMID: 11691934

bioRxiv preprint doi: https://doi.org/10.1101/481457; this version posted December 26, 2018. The copyright holder for this preprint (which was not certified by peer review) is the author/funder. All rights reserved. No reuse allowed without permission.

Bowers EM, Yan G, Mukherjee C, Orry A, Wang L, Holbert MA, Crump NT, Hazzalin CA, Liszczak G, Yuan H, Larocca C, Saldanha SA, Abagyan R, Sun Y, Meyers DJ, Marmorstein R, Mahadevan LC, Alani RM, Cole PA. Virtual ligand screening of the p300/CBP histone acetyltransferase: identification of a selective small molecule inhibitor. Chem Biol. 2010 May 28;17(5):471-82. doi: 10.1016/j.chembiol.2010.03.006. PMID: 20534345

Brüschweiler S, Konrat R, Tollinger M. Allosteric communication in the KIX domain proceeds through dynamic repacking of the hydrophobic core. ACS Chem Biol. 2013 Jul 19;8(7):1600-10. doi: 10.1021/cb4002188. Epub 2013 May 20.

Bürckstümmer T, Bennett KL, Preradovic A, Schütze G, Hantschel O, Superti-Furga G, Bauch A. An efficient tandem affinity purification procedure for interaction proteomics in mammalian cells. Nat Methods. 2006 3:1013-9. PMID: 17060908

Budzyński MA, Puustinen MC, Joutsen J, Sistonen L. Uncoupling Stress-Inducible Phosphorylation of Heat Shock Factor 1 from Its Activation. Mol Cell Biol. 2015 Jul;35(14):2530-40. doi: 10.1128/MCB.00816-14. Epub 2015 May 11. PMID: 25963659

Campbell KM, Lumb KJ. Structurally distinct modes of recognition of the KIX domain of CBP by Jun and CREB. Biochemistry. 2002 Nov 26;41(47):13956-64. PMID: 12437352

Chan HM, La Thangue NB. p300/CBP proteins: HATs for transcriptional bridges and scaffolds. J Cell Sci. 2001 Jul;114(Pt 13):2363-73. PMID: 11559745

Chang Y, Ostling P, Akerfelt M, Trouillet D, Rallu M, Gitton Y, El Fatimy R, Fardeau V, Le Crom S, Morange M, Sistonen L, Mezger V. Role of heat-shock factor 2 in cerebral cortex formation and as a regulator of p35 expression. Genes Dev. 2006 Apr 1;20(7):836-47. PMID: 16600913

Cook PR, Polakowski N, Lemasson I. HTLV-1 HBZ protein deregulates interactions between cellular factors and the KIX domain of p300/CBP. J Mol Biol. 2011 Jun 10;409(3):384-98. doi: 10.1016/j.jmb.2011.04.003. Epub 2011 Apr 8. PMID: 21497608

Dai C, Whitesell L, Rogers AB, Lindquist S. Heat shock factor 1 is a powerful multifaceted modifier of carcinogenesis. Cell. 2007 Sep 21;130(6):1005-18. PMID: 17889646

Dancy BM, Cole PA. Protein lysine acetylation by p300/CBP. Chem Rev. 2015 Mar 25;115(6):2419-52. doi: 10.1021/cr500452k. Epub 2015 Jan 16. PMID: 25594381 - Erratum 27304234.

Duval R, Fritsch L, Bui LC, Berthelet J, Guidez F, Mathieu C, Dupret JM, Chomienne C, Ait-Si-Ali S, Rodrigues-Lima F. An acetyltransferase assay for CREB-binding protein based on reverse phase-ultra-fast liquid chromatography of fluorescent histone H3 peptides. Anal Biochem. 2015 Oct 1;486:35-7. doi: 10.1016/j.ab.2015.06.024. PMID: 26099937

Delvecchio M, Gaucher J, Aguilar-Gurrieri C, Ortega E, Panne D. Structure of the p300 catalytic core and implications for chromatin targeting and HAT regulation. Nat Struct Mol Biol. 2013 Sep;20(9):1040-6. doi: 10.1038/nsmb.2642. PMID: 23934153

El Fatimy R, Miozzo F, Le Mouël A, Abane R, Schwendimann L, Sabéran-Djoneidi D, de Thonel A, Massaoudi I, Paslaru L, Hashimoto-Torii K, Christians E, Rakic P, Gressens P, Mezger V. Heat shock factor 2 is a stress-responsive mediator of neuronal migration defects in models of fetal alcohol

bioRxiv preprint doi: https://doi.org/10.1101/481457; this version posted December 26, 2018. The copyright holder for this preprint (which was not certified by peer review) is the author/funder. All rights reserved. No reuse allowed without permission.

syndrome. EMBO Mol Med. 2014 Aug;6(8):1043-61. doi: 10.15252/emmm.201303311. PMID: 25027850

Elsing AN, Aspelin C, Björk JK, Bergman HA, Himanen SV, Kallio MJ, Roos-Mattjus P, Sistonen L. Expression of HSF2 decreases in mitosis to enable stress-inducible transcription and cell survival. J Cell Biol. 2014 Sep 15;206(6):735-49. doi: 10.1083/jcb.201402002. Epub 2014 Sep 8. PMID: 25202032

Geng H, Liu Q, Xue C, David LL, Beer TM, Thomas GV, Dai MS, Qian DZ. HIF1α protein stability is increased by acetylation at lysine 709. J Biol Chem. 2012 Oct 12;287(42):35496-505. doi: 10.1074/jbc.M112.400697. Epub 2012 Aug 20. PMID: 22908229

Gomez-Pastor R, Burchfiel ET, Neef DW, Jaeger AM, Cabiscol E, McKinstry SU, Doss A, Aballay A, Lo DC, Akimov SS, Ross CA, Eroglu C, Thiele DJ. Abnormal degradation of the neuronal stress-protective transcription factor HSF1 in Huntington's disease. Nat Commun. 2017 Feb 13;8:14405. doi: 10.1038/ncomms14405. PMID: 28194040

Gomez-Pastor R, Burchfiel ET, Thiele DJ. Regulation of heat shock transcription factors and their roles in physiology and disease. Nat Rev Mol Cell Biol. 2018 Jan;19(1):4-19. doi: 10.1038/nrm.2017.73. Epub 2017 Aug 30. Review. PMID: 28852220

Goto NK, Zor T, Martinez-Yamout M, Dyson HJ, Wright PE. Cooperativity in transcription factor binding to the coactivator CREB-binding protein (CBP). The mixed lineage leukemia protein (MLL) activation domain binds to an allosteric site on the KIX domain. J Biol Chem. 2002 Nov 8;277(45):43168-74. Epub 2002 Aug 29. PMID: 12205094

Grossman SR, Deato ME, Brignone C, Chan HM, Kung AL, Tagami H, Nakatani Y, Livingston DM. Polyubiquitination of p53 by a ubiquitin ligase activity of p300. Science. 2003 Apr 11;300(5617):342-4. DOI: 10.1126/science.1080386. PMID: 12690203

Hartl FU, Bracher A, Hayer-Hartl M. Molecular chaperones in protein folding and proteostasis. Nature. 2011 Jul 20;475(7356):324-32. doi: 10.1038/nature10317. PMID: 21776078

Herce HD, Deng W, Helma J, Leonhardt H, Cardoso MC. Visualization and targeted disruption of protein interactions in living cells. Nat Commun. 2013;4:2660. PMID: 24154492

Herriot R, Miedzybrodzka Z2. Antibody deficiency in Rubinstein-Taybi syndrome. Clin Genet. 2016 Mar;89(3):355-8. doi: 10.1111/cge.12671. Epub 2015 Sep 28. PMID: 26307339

Huttlin EL, Ting L, Bruckner RJ, Gebreab F, Gygi MP, Szpyt J, Tam S, Zarraga G, Colby G, Baltier K, Dong R, Guarani V, Vaites LP, Ordureau A, Rad R, Erickson BK, Wühr M, Chick J, Zhai B, Kolippakkam D, Mintseris J, Obar RA, Harris T, Artavanis-Tsakonas S, Sowa ME, De Camilli P, Paulo JA, Harper JW, Gygi SP. The BioPlex Network: A Systematic Exploration of the Human Interactome. Cell. 2015 Jul 16;162(2):425-440. doi: 10.1016/j.cell.2015.06.043. PMID: 26186194

Jain S, Wei J, Mitrani LR, Bishopric NH. Auto-acetylation stabilizes p300 in cardiac myocytes during acute oxidative stress, promoting STAT3 accumulation and cell survival. Breast Cancer Res Treat. 2012 Aug;135(1):103-14. doi: 10.1007/s10549-012-2069-6. Epub 2012 May 5. PMID: 22562121

Jiang YQ, Wang XL, Cao XH, Ye ZY, Li L, Cai WQ. Increased heat shock transcription factor 1 in the cerebellum reverses the deficiency of Purkinje cells in Alzheimer's disease. Brain Res. 2013 Jun 26;1519:105-11. doi: 10.1016/j.brainres.2013.04.059. Epub 2013 May 9. PMID: 23665061

bioRxiv preprint doi: https://doi.org/10.1101/481457; this version posted December 26, 2018. The copyright holder for this preprint (which was not certified by peer review) is the author/funder. All rights reserved. No reuse allowed without permission.

Jolly C, Metz A, Govin J, Vigneron M, Turner BM, Khochbin S, Vourc'h C. Stress-induced transcription of satellite III repeats. J Cell Biol. 2004 Jan 5;164(1):25-33. Epub 2003 Dec 29. PMID: 14699086

Jolly C, Morimoto R, Robert-Nicoud M, Vourc'h C. HSF1 transcription factor concentrates in nuclear foci during heat shock: relationship with transcription sites. J Cell Sci. 1997 Dec;110 (Pt 23):2935-41. PMID: 9359877

Jolly C, Usson Y, Morimoto RI. Rapid and reversible relocalization of heat shock factor 1 within seconds to nuclear stress granules. Proc Natl Acad Sci U S A. 1999 Jun 8;96(12):6769-74. PMID: 10359787

Kallio M, Chang Y, Manuel M, Alastalo TP, Rallu M, Gitton Y, Pirkkala L, Loones MT, Paslaru L, Larney S, Hiard S, Morange M, Sistonen L, Mezger V. Brain abnormalities, defective meiotic chromosome synapsis and female subfertility in HSF2 null mice. EMBO J. 2002 Jun 3;21(11):2591-601. DOI: 10.1093/emboj/21.11.2591. PMID: 12032072

Kalkhoven E, Roelfsema JH, Teunissen H, den Boer A, Ariyurek Y, Zantema A, Breuning MH, Hennekam RC, Peters DJ. Loss of CBP acetyltransferase activity by PHD finger mutations in Rubinstein-Taybi syndrome. Hum Mol Genet. 2003 Feb 15;12(4):441-50. PMID: 12566391

Kalkhoven E, Teunissen H, Houweling A, Verrijzer CP, Zantema A.The PHD type zinc finger is an integral part of the CBP acetyltransferase domain. Mol Cell Biol. 2002 Apr;22(7):1961-70. PMID: 11884585

Kawasaki H, Eckner R, Yao TP, Taira K, Chiu R, Livingston DM, Yokoyama KK. Distinct roles of the co-activators p300 and CBP in retinoic-acid-induced F9-cell differentiation. Nature. 1998 May 21;393(6682):284-9. PMID: 9607768

Kawazoe Y, Nakai A, Tanabe M, Nagata K. Proteasome inhibition leads to the activation of all members of the heat-shock-factor family. Eur J Biochem. 1998 Jul 15;255(2):356-62. PMID: 9716376

Kim W, Bennett EJ, Huttlin EL, Guo A, Li J, Possemato A, Sowa ME, Rad R, Rush J, Comb MJ, Harper JW, Gygi SP. Systematic and quantitative assessment of the ubiquitin-modified proteome. Mol Cell. 2011 Oct 21;44(2):325-40. doi: 10.1016/j.molcel.2011.08.025. Epub 2011 Sep 8. PMID: 21906983

Kim E, Wang B, Sastry N, Masliah E, Nelson PT, Cai H, Liao FF. NEDD4-mediated HSF1 degradation underlies α-synucleinopathy. Hum Mol Genet. 2016 Jan 15;25(2):211-22. doi: 10.1093/hmg/ddv445. Epub 2015 Oct 26. PMID: 26503960

Kobayashi A, Numayama-Tsuruta K, Sogawa K, Fujii-Kuriyama Y. CBP/p300 functions as a possible transcriptional coactivator of Ah receptor nuclear translocator (Arnt). J Biochem (Tokyo) 1997; 122:703-10. PMID: 9399571

Lamparter CL, Winn LM. Valproic acid exposure decreases Cbp/p300 protein expression and histone acetyltransferase activity in P19 cells. Toxicol Appl Pharmacol. 2016 Sep 1;306:69-78. doi: 10.1016/j.taap.2016.07.001. PMID: 27381264

Lancaster MA, Renner M, Martin CA, Wenzel D, Bicknell LS, Hurles ME, Homfray T, Penninger JM, Jackson AP, Knoblich JA. Cerebral organoids model human brain development and microcephaly. Nature. 2013 Sep 19;501(7467):373-9. doi: 10.1038/nature12517. Epub 2013 Aug 28. PMID: 23995685

bioRxiv preprint doi: https://doi.org/10.1101/481457; this version posted December 26, 2018. The copyright holder for this preprint (which was not certified by peer review) is the author/funder. All rights reserved. No reuse allowed without permission.

Lee CW, Arai M, Martinez-Yamout MA, Dyson HJ, Wright PE. Mapping the interactions of the p53 transactivation domain with the KIX domain of CBP. Biochemistry. 2009 Mar 17;48(10):2115-24. doi: 10.1021/bi802055v. PMID: 19220000

Marinova Z, Ren M, Wendland JR, Leng Y, Liang MH, Yasuda S, Leeds P, Chuang DM. Valproic acid induces functional heat-shock protein 70 via Class I histone deacetylase inhibition in cortical neurons: a potential role of Sp1 acetylation. J Neurochem. 2009 Nov;111(4):976-87. doi: 10.1111/j.1471-4159.2009.06385.x. PMID: 19765194

Mashiach E, Schneidman-Duhovny D, Andrusier N, Nussinov R, Wolfson HJ. FireDock: a web server for fast interaction refinement in molecular docking. Nucleic Acids Res. 2008 Jul 1;36(Web Server issue):W229-32. doi: 10.1093/nar/gkn186. Epub 2008 Apr 19. PMID: 18424796

Mathew A, Mathur SK, Morimoto RI. Heat shock response and protein degradation: regulation of HSF2 by the ubiquitin-proteasome pathway. Mol Cell Biol. 1998 Sep;18(9):5091-8. PMID: 9710593

McMillan DR, Xiao X, Shao L, Graves K, Benjamin IJ. Targeted disruption of heat shock transcription factor 1 abolishes thermotolerance and protection against heat-inducible apoptosis. J Biol Chem. 1998 Mar 27;273(13):7523-8. PMID: 9516453

Mendillo ML, Santagata S, Koeva M, Bell GW, Hu R, Tamimi RM, Fraenkel E, Ince TA, Whitesell L, Lindquist S. HSF1 drives a transcriptional program distinct from heat shock to support highly malignant human cancers. Cell. 2012 Aug 3;150(3):549-62. doi: 10.1016/j.cell.2012.06.031. PMID: 22863008

Miozzo F, Sabéran-Djoneidi D, Mezger V. HSFs, Stress Sensors and Sculptors of Transcription Compartments and Epigenetic Landscapes. J Mol Biol. 2015 Dec 4;427(24):3793-816. doi: 10.1016/j.jmb.2015.10.007. Epub 2015 Oct 22. PMID 26482101

Neef DW, Jaeger AM, Thiele DJ. Heat shock transcription factor 1 as a therapeutic target in neurodegenerative diseases. Nat Rev Drug Discov. 2011 Dec 1;10(12):930-44. doi: 10.1038/nrd3453. Review. PMID: 22129991

Naimi DR, Munoz J, Rubinstein J, Hostoffer RW Jr. Rubinstein-Taybi syndrome: an immune deficiency as a cause for recurrent infections. Allergy Asthma Proc. 2006 May-Jun;27(3):281-4. PMID: 16913274

Nakai, A (ed.) Heat Shock Factor. (Springer, 2016).

Östling P, Björk JK, Roos-Mattjus P, Mezger V, Sistonen L. Heat shock factor 2 (HSF2) contributes to inducible expression of hsp genes through interplay with HSF1. J Biol Chem. 2007 Mar 9;282(10):7077-86. Epub 2007 Jan 9. PMID: 17213196

Parker D, Ferreri K, Nakajima T, LaMorte VJ, Evans R, Koerber SC, Hoeger C, Montminy MR.Pierce BG, Phosphorylation of CREB at Ser-133 induces complex formation with CREB-binding protein via a direct mechanism. Mol Cell Biol. 1996 Feb;16(2):694-703. PMID: 8552098

Partanen A, Motoyama J, Hui CC. Developmentally regulated expression of the transcriptional cofactors/histone acetyltransferases CBP and p300 during mouse embryogenesis. Int J Dev Biol. 1999 Sep;43(6):487-94. PMID: 10610021

bioRxiv preprint doi: https://doi.org/10.1101/481457; this version posted December 26, 2018. The copyright holder for this preprint (which was not certified by peer review) is the author/funder. All rights reserved. No reuse allowed without permission.

Rack JG, Lutter T, Kjæreng Bjerga GE, Guder C, Ehrhardt C, Värv S, Ziegler M, Aasland R. The PHD finger of p300 influences its ability to acetylate histone and non-histone targets. J Mol Biol. 2014 Dec 12;426(24):3960-72. doi: 10.1016/j.jmb.2014.08.011. PMID: 25158095

Rallu M, Loones M, Lallemand Y, Morimoto R, Morange M, Mezger V. Function and regulation of heat shock factor 2 during mouse embryogenesis. Proc Natl Acad Sci U S A. 1997 Mar 18;94(6):2392-7. PMID: 9122205

Ramachandran GN, Ramakrishnan C, Sasisekharan V (1963). Stereochemistry of polypeptide chain configurations. Journal of Molecular Biology. 7: 95–9. PMID: 13990617

Raychaudhuri S, Loew C, Körner R, Pinkert S, Theis M, Hayer-Hartl M, Buchholz F, Hartl FU. Interplay of acetyltransferase EP300 and the proteasome system in regulating heat shock transcription factor 1. Cell. 2014 Feb 27;156(5):975-85. doi: 10.1016/j.cell.2014.01.055. PMID: 24581496

Rizzi N, Denegri M, Chiodi I, Corioni M, Valgardsdottir R, Cobianchi F, Riva S, Biamonti G. Transcriptional activation of a constitutive heterochromatic domain of the human genome in response to heat shock. Mol Biol Cell. 2004 Feb;15(2):543-51. Epub 2003 Nov 14. PMID: 14617804

Rothbauer U, Zolghadr K, Muyldermans S, Schepers A, Cardoso MC, Leonhardt H. A versatile nanotrap for biochemical and functional studies with fluorescent fusion proteins. Mol Cell Proteomics. 2008 Feb;7(2):282-9. Epub 2007 Oct 21. PMID: 17951627

Sandqvist A, Björk JK, Akerfelt M, Chitikova Z, Grichine A, Vourc'h C, Jolly C, Salminen TA, Nymalm Y, Sistonen L. Heterotrimerization of heat-shock factors 1 and 2 provides a transcriptional switch in response to distinct stimuli. Mol Biol Cell. 2009 Mar;20(5):1340-7. doi: 10.1091/mbc.E08-08-0864. Epub 2009 Jan 7. PMID: 19129477

Sanial M, Bécam I, Hofmann L, Behague J, Argüelles C, Gourhand V, Bruzzone L, Holmgren RA, Plessis A. Dose-dependent transduction of Hedgehog relies on phosphorylation-based feedback between the G-protein-coupled receptor Smoothened and the kinase Fused. Development. 2017 May 15;144(10):1841-1850. doi: 10.1242/dev.144782. PMID: 28360132

Santagata S, Hu R, Lin NU, Mendillo ML, Collins LC, Hankinson SE, Schnitt SJ, Whitesell L, Tamimi RM, Lindquist S, Ince TA. High levels of nuclear heat-shock factor 1 (HSF1) are associated with poor prognosis in breast cancer. Proc Natl Acad Sci U S A. 2011 Nov 8;108(45):18378-83. doi: 10.1073/pnas.1115031108. Epub 2011 Oct 31. PMID: 22042860

Santagata S, Mendillo ML, Tang YC, Subramanian A, Perley CC, Roche SP, Wong B, Narayan R, Kwon H, Koeva M, Amon A, Golub TR, Porco JA Jr, Whitesell L, Lindquist S. Tight coordination of protein translation and HSF1 activation supports the anabolic malignant state. Science. 2013 Jul 19;341(6143):1238303. doi: 10.1126/science.1238303. PMID: 23869022

Sankar N, Baluchamy S, Kadeppagari RK, Singhal G, Weitzman S, Thimmapaya B. p300 provides a corepressor function by cooperating with YY1 and HDAC3 to repress c-Myc. Oncogene. 2008 Sep 25;27(43):5717-28. doi: 10.1038/onc.2008.181. PMID: 18542060

Sarge KD, Murphy SP, Morimoto RI. Mol Cell Biol. 1993 Mar;13(3):1392-407. Activation of heat shock gene transcription by heat shock factor 1 involves oligomerization, acquisition of DNA-binding activity, and nuclear localization and can occur in the absence of stress. PMID: 8441385

bioRxiv preprint doi: https://doi.org/10.1101/481457; this version posted December 26, 2018. The copyright holder for this preprint (which was not certified by peer review) is the author/funder. All rights reserved. No reuse allowed without permission.

Schneidman-Duhovny D, Inbar Y, Nussinov R, Wolfson HJ. PatchDock and SymmDock: servers for rigid and symmetric docking. Nucleic Acids Res. 2005 Jul 1;33(Web Server issue):W363-7. PMID: 15980490

Sierra J, Yoshida T, Joazeiro CA, Jones KA. The APC tumor suppressor counteracts beta-catenin activation and H3K4 methylation at Wnt target genes. Genes Dev. 2006 Mar 1;20(5):586-600. DOI: 10.1101/gad.1385806. PMID: 16510874

Sistonen L, Sarge KD, Phillips B, Abravaya K, Morimoto RI. Activation of heat shock factor 2 during hemin-induced differentiation of human erythroleukemia cells. Mol Cell Biol. 1992 Sep;12(9):4104-11. PMID: 1508207

Spena S, Gervasini C, Milani D. Ultra-Rare Syndromes: The Example of Rubinstein-Taybi Syndrome. J Pediatr Genet. 2015a Sep;4(3):177-86. doi: 10.1055/s-0035-1564571. Epub 2015 Sep 28. Review. PMID: 27617129

Spena S, Milani D, Rusconi D, Negri G, Colapietro P, Elcioglu N, Bedeschi F, Pilotta A, Spaccini L, Ficcadenti A, Magnani C, Scarano G, Selicorni A, Larizza L, Gervasini C. Insights into genotype-phenotype correlations from CREBBP point mutation screening in a cohort of 46 Rubinstein-Taybi syndrome patients. Clin Genet. 2015b Nov;88(5):431-40. doi: 10.1111/cge.12537. PMID: 25388907

Takii R, Fujimoto M, Tan K, Takaki E, Hayashida N, Nakato R, Shirahige K, Nakai A. ATF1 modulates the heat shock response by regulating the stress-inducible heat shock factor 1 transcription complex. Mol Cell Biol. 2015 Jan;35(1):11-25. doi: 10.1128/MCB.00754-14. Epub 2014 Oct 13. PMID: 25312646

Tang S, Chen H, Cheng Y, Nasir MA, Kemper N, Bao E. The interactive association between heat shock factor 1 and heat shock proteins in primary myocardial cells subjected to heat stress. Int J Mol Med. 2016 Jan;37(1):56-62. doi: 10.3892/ijmm.2015.2414. PMID: 26719858

Thakur JK, Yadav A, Yadav G. Molecular recognition by the KIX domain and its role in gene regulation. Nucleic Acids Res. 2014 Feb;42(4):2112-25. doi: 10.1093/nar/gkt1147. Epub 2013 Nov 18. PMID: 24253305

Turnell AS, Stewart GS, Grand RJ, Rookes SM, Martin A, Yamano H, Elledge SJ, Gallimore PH. The APC/C and CBP/p300 cooperate to regulate transcription and cell-cycle progression. Nature. 2005 Dec 1;438(7068):690-5. PMID: 16319895

Vecsey CG, Hawk JD, Lattal KM, Stein JM, Fabian SA, Attner MA, Cabrera SM, McDonough CB,Brindle PK, Abel T, Wood MA. Histone deacetylase inhibitors enhance memory and synaptic plasticity via CREB:CBP-dependent transcriptional activation. J Neurosci 2007;27:6128–6140. PubMed: 17553985

Vihervaara A, Sergelius C, Vasara J, Blom MA, Elsing AN, Roos-Mattjus P, Sistonen L. Transcriptional response to stress in the dynamic chromatin environment of cycling and mitotic cells. Proc Natl Acad Sci U S A. 2013 Sep 3;110(36):E3388-97. doi: 10.1073/pnas.1305275110. PMID: 23959860

Vihervaara A, Sistonen L. HSF1 at a glance. J Cell Sci. 2014 Jan 15;127(Pt 2):261-6. doi: 10.1242/jcs.132605. PMID: 24421309

Wagner SA, Beli P, Weinert BT, Nielsen ML, Cox J, Mann M, Choudhary C. A proteome-wide, quantitative survey of in vivo ubiquitylation sites reveals widespread regulatory roles. Mol Cell Proteomics. 2011 Oct;10(10):M111.013284. doi: 10.1074/mcp.M111.013284. Epub 2011 Sep 1. PMID: 21890473

bioRxiv preprint doi: https://doi.org/10.1101/481457; this version posted December 26, 2018. The copyright holder for this preprint (which was not certified by peer review) is the author/funder. All rights reserved. No reuse allowed without permission.

Wang F, Marshall CB, Yamamoto K, Li GY, Gasmi-Seabrook GM, Okada H, Mak TW, Ikura M. Structures of KIX domain of CBP in complex with two FOXO3a transactivation domains reveal promiscuity and plasticity in coactivator recruitment. Proc Natl Acad Sci U S A. 2012 Apr 17;109(16):6078-83. doi: 10.1073/pnas.1119073109. Epub 2012 Apr 2. PMID: 22474372

Wang G, Zhang J, Moskophidis D, Mivechi NF. Targeted disruption of the heat shock transcription factor (hsf)-2 gene results in increased embryonic lethality, neuronal defects, and reduced spermatogenesis. Genesis. 2003 May;36(1):48-61. PMID: 12748967

Wang X, Asea A, Xie Y, Kabingu E, Stevenson MA, Calderwood SK. RSK2 represses HSF1 activation during heat shock. Cell Stress Chaperones. 2000 Nov; 5(5): 432–437. PMID: 11189448

Westerheide SD, Anckar J, Stevens SM Jr, Sistonen L, Morimoto RI. Stress-inducible regulation of heat shock factor 1 by the deacetylase SIRT1. Science. 2009 Feb 20;323(5917):1063-6. doi: 10.1126/science.1165946. Erratum in: Science. 2013 Nov 22;342(6161):931. PMID: 19229036

Wiehe K, Hwang H, Kim BH, Vreven T, Weng Z. ZDOCK server: interactive docking prediction of protein-protein complexes and symmetric multimers. Bioinformatics. 2014 Jun 15;30(12):1771-3. doi: 10.1093/bioinformatics/btu097. Epub 2014 Feb 14. PMID: 24532726

Wu C. Heat shock transcription factors: structure and regulation. Annu Rev Cell Dev Biol. 1995. PMID: 8689565

Xiao X, Zuo X, Davis AA, McMillan DR, Curry BB, Richardson JA, Benjamin IJ. HSF1 is required for extra-embryonic development, postnatal growth and protection during inflammatory responses in mice. EMBO J. 1999 Nov 1;18(21):5943-52. PMID: 10545106

Xu D, Zalmas LP, and Nicholas B La Thangue NB. A transcription cofactor required for the heat-shock response. EMBO Rep. 2008 Jul; 9(7): 662–669. PMID: 18451878

Yang XJ, Seto E. Lysine acetylation: codified crosstalk with other posttranslational modifications. Mol Cell. 2008 Aug 22;31(4):449-61. doi: 10.1016/j.molcel.2008.07.002. PMID: 18722172

Yao TP, Oh SP, Fuchs M, Zhou ND, Ch'ng LE, Newsome D, Bronson RT, Li E, Livingston DM, Eckner R. Gene dosage-dependent embryonic development and proliferation defects in mice lacking the transcriptional integrator p300. Cell. 1998 May 1;93(3):361-72. PMID: 9590171

Yehezkel S, Segev Y, Viegas-Péquignot E, Skorecki K, Selig S. Hypomethylation of subtelomeric regions in ICF syndrome is associated with abnormally short telomeres and enhanced transcription from telomeric regions. Hum Mol Genet. 2008 Sep 15;17(18):2776-89. doi: 10.1093/hmg/ddn177. Epub 2008 Jun 16. PMID: 18558631

Yoshima T, Yura T, Yanagi H.The trimerization domain of human heat shock factor 2 is able to interact with nucleoporin p62. Biochem Biophys Res Commun. 1997 Nov 7;240(1):228-33. PMID: 9367915

Zelin E, Zhang Y, Toogun OA, Zhong S, Freeman BC. The p23 molecular chaperone and GCN5 acetylase jointly modulate protein-DNA dynamics and open chromatin status. Mol Cell. 2012 Nov 9;48(3):459-70. doi: 10.1016/j.molcel.2012.08.026. Epub 2012 Sep 27. PMID: 23022381

Zor T, De Guzman RN, Dyson HJ, Wright PE. Solution structure of the KIX domain of CBP bound to the transactivation domain of c-Myb. J Mol Biol. 2004 Mar 26;337(3):521-34. PMID: 15019774

bioRxiv preprint doi: https://doi.org/10.1101/481457; this version posted December 26, 2018. The copyright holder for this preprint (which was not certified by peer review) is the author/funder. All rights reserved. No reuse allowed without permission.

Supplementary references

Abravaya K, Phillips B, Morimoto RI. Heat shock-induced interactions of heat shock transcription factor and the human hsp70 promoter examined by in vivo footprinting. Mol Cell Biol. 1991 Jan;11(1):586-92. PMID: 1986252

Bordoli L, Hüsser S, Lüthi U, Netsch M, Osmani H, Eckner R. Functional analysis of the p300 acetyltransferase domain: the PHD finger of p300 but not of CBP is dispensable for enzymatic activity. Nucleic Acids Res. 2001 Nov 1;29(21):4462-71. PMID: 11691934

Cerisier N, Regad L, Triki D, Camproux AC, Petitjean M. Cavity Versus Ligand Shape Descriptors: Application to Urokinase Binding Pockets. J Comput Biol. 2017 Nov;24(11):1134-1137. doi: 10.1089/cmb.2017.0061. Epub 2017 Jun 1. PMID: 28570103

Cong L, Ran FA, Cox D, Lin S, Barretto R, Habib N, Hsu PD, Wu X, Jiang W, Marraffini LA, Zhang F. Multiplex genome engineering using CRISPR/Cas systems. Science. 2013 Feb 15;339(6121):819-23. doi: 10.1126/science.1231143. PMID: 23287718

El Fatimy R, Miozzo F, Le Mouël A, Abane R, Schwendimann L, Sabéran-Djoneidi D, de Thonel A, Massaoudi I, Paslaru L, Hashimoto-Torii K, Christians E, Rakic P, Gressens P, Mezger V. Heat shock factor 2 is a stress-responsive mediator of neuronal migration defects in models of fetal alcohol syndrome. EMBO Mol Med. 2014 Aug;6(8):1043-61. doi: 10.15252/emmm.201303311. PMID: 25027850

Fritsch L, Robin P, Mathieu JR, Souidi M, Hinaux H, Rougeulle C, Harel-Bellan A, Ameyar-Zazoua M, Ait-Si-Ali S. A subset of the histone H3 lysine 9 methyltransferases Suv39h1, G9a, GLP, and SETDB1 participate in a multimeric complex. Mol Cell. 2010 Jan 15;37(1):46-56. doi: 10.1016/j.molcel.2009.12.017. PMID: 20129054

Mosser DD, Theodorakis NG, Morimoto RI. Coordinate changes in heat shock element-binding activity and HSP70 gene transcription rates in human cells. Mol Cell Biol. 1988 Nov;8(11):4736-44. PMID: 3211126

Pirkkala L, Alastalo TP, Zuo X, Benjamin IJ, Sistonen L. Disruption of heat shock factor 1 reveals an essential role in the ubiquitin proteolytic pathway. Mol Cell Biol. 2000 Apr;20(8):2670-5. PMID: 10733569

Sandqvist A, Björk JK, Akerfelt M, Chitikova Z, Grichine A, Vourc'h C, Jolly C, Salminen TA, Nymalm Y, Sistonen L. Heterotrimerization of heat-shock factors 1 and 2 provides a transcriptional switch in response to distinct stimuli. Mol Biol Cell. 2009. 20:1340-7. PMID: 19129477

Sandrin V, Cosset FL (2006) Intracellular versus cell surface assembly of retroviral pseudotypes is determined by the cellular localization of the viral glycoprotein, its capacity to interact with Gag, and the expression of the Nef protein. J Biol Chem 281: 528-542. PMID: 16195228

Schneidman-Duhovny D, Inbar Y, Nussinov R, Wolfson HJ. PatchDock and SymmDock: servers for rigid and symmetric docking. Nucleic Acids Res. 2005 Jul 1;33(Web Server issue):W363-7. PMID: 15980490

Shu W, Ji H, Lu M. Trimerization specificity in HIV-1 gp41: analysis with a GCN4 leucine zipper model. Biochemistry. 1999 Apr 27;38(17):5378-85. DOI: 10.1021/bi990199w. PMID: 10220324

bioRxiv preprint doi: https://doi.org/10.1101/481457; this version posted December 26, 2018. The copyright holder for this preprint (which was not certified by peer review) is the author/funder. All rights reserved. No reuse allowed without permission.

Shu W, Liu J, Ji H, Lu M. Core structure of the outer membrane lipoprotein from Escherichia coli at 1.9 A resolution. J Mol Biol. 2000 Jun 16;299(4):1101-12. DOI: 10.1006/jmbi.2000.3776. PMID: 10843861

Yahi H, Fritsch L, Philipot O, Guasconi V, Souidi M, Robin P, Polesskaya A, Losson R, Harel-Bellan A, Ait-Si-Ali S. Differential cooperation between heterochromatin protein HP1 isoforms and MyoD in myoblasts. J Biol Chem. 2008 Aug 29;283(35):23692-700. doi: 10.1074/jbc.M802647200. PMID: 18599480

bioRxiv preprint doi: https://doi.org/10.1101/481457; this version posted December 26, 2018. The copyright holder for this preprint (which was not certified by peer review) is the author/funder. All rights reserved. No reuse allowed without permission.

EXPERIMENTAL PROCEDURES

CONTACT FOR REAGENT AND RESOURCE SHARING

More detailed information and requests for resources and reagents should be directed to and will be fulfilled by the co-corresponding authors: Aurélie de THONEL (aurelie.dethonel@univ-paris-diderot.fr), Lea SISTONEN (lea.sistonen@btk.fi), and Valérie MEZGER (valerie.mezger@univ-apris-diderot.fr).

Reagents and treatments

Proteasome inhibitor MG132 was used for 6h (N2A, U20S) at a final concentration of 20µM. HDACs inhibitor VPA (Interchim, AYJ060) was used at 1 mM for 3 h. The HAT inhibitor C646 (Sigma-Aldrich; SML0002) was used at a final concentration of 20 or 40 µM for 4h. For all chemicals, DMSO was used as vehicle (control).

Heat shock treatments were performed in water bath at 42 or 43°C for the indicated times.

Table for antibodies

Antibodies	species	Clone	reference	Manufacturer	WB	IP	ImmunoF	IHC
Acetyl-lysine (Pan)	rabbit	pAb	#9441	Cell signalling Technology	1/1000		1/1000	
Actin	mouse	AC40	A3853	Sigma-Aldrich	1/4000			
Alexa Fluor 488	Donkey anti-mouse		715-546-151	J.ImmunoRes			1/800	1/800
Alexa Fluor 488	goat anti-rabbit		A-11008	J.ImmunoRes			1/800	1/800
Alexa Fluor 594	goat anti-rabbit		A-11037	J.ImmunoRes			1/800	1/800
CBP	rabbit IgG	D6C5	#7389	Cell signalling Technology	1/1000		1/100	
CBP	rabbit	A-22	sc-369	Santa-Cruz	1/1000			1/100
Cy3TM-3	Donkey anti-mouse		715-165-150	J.ImmunoRes			1/800	1/800
EP300	rabbit	pAb	sc-584	Santa-Cruz	1/500		1/25	1/25
Flag tag	mouse	M2	F1804	Sigma-Aldrich	1/1000	2µg		
GFP tag	mouse	IgG1	MAB2510	Millipore	1/1000			
GFP-Trap-A	mouse		gta-20	chromotek		25µl		
GST tag	mouse	IgG	AE001	Ab Clonal	1/2000	2,5µl		
H3K18Ac	rabbit	pAb	GTX128943-S	Euromedex				
H3K27Ac	rabbit	pAb	pAb174050	Diagenode	1/1000			
HDAC1	rabbit	pAb	7028	Abcam	1/4000		1/900	
HDAC2	rabbit	pAb	7029	Abcam	1/4000			
HRP mouse Fab	Goat anti-mouse	F(ab')2	115 036 072	J.ImmunoRes	1/50 000			
HRP rabbit				J.ImmunoRes	1/50 000			
HSC70	rat	mAb	ADI-SPA-815	Stressgen	1/1000			
HSF1	rabbit	pAb	#4356	Cell signalling Technology	1/1000		1/800	
HSF2	mouse	G11	sc-74529	Santa-Cruz	1/250	4µg		
HSF2	mouse	3E2	ab69621	abcam		4µg		
HSF2	rabbit	pAb	H57	Lea Sistonen Lab			1/600	1/600
HSP70	mouse		ADI-SPA-810	Stressgen	1/1000			
IgG	mouse		I5381	sigma-Aldrich				
Myc tag	mouse	9B11	#2276	Cell signalling Technology	1/1000			
Myc-Trap-A	mouse		yta-20	chromotek		25µl		
Snap	rabbit	pAb	P9310	NEB	1/1000			
Sox 2	rabbit	pAb	ab97959	abcam				1/500
Trap-A CTL	mouse		bab-20	Chromotek		25µl		

Plasmid Table and constructs

bioRxiv preprint doi: https://doi.org/10.1101/481457; this version posted December 26, 2018. The copyright holder for this preprint (which was not certified by peer review) is the author/funder. All rights reserved. No reuse allowed without permission.

Plasmid name	Reference	vector	Origin	Supplier
Cas9 guide RNA HSF2	Cong et al., 2013	pX300 Cas9	human	
CBP DN-HA				
CBP-HA	kind gift of Pr. Wei Gu	pcDNA3-CMV	mouse	
EP300-HA	kind gift from W Sellers (East Tennessee State University, USA); Duval et al., 2015	1246 pCMVb MycHA	human	Addgene # U10718
GFP binder nanobody (GBP)	Kind gift from P.A. Defossez (University Paris-Diderot, France); Zolghadr et al., 2008			
GFP tag		pEGFP-N1		Clontech (6085-1)
HDAC1 DN(D181A)-Flag	Kuzmochka et al., 2014	pcDNA3.1	human	
HDAC1-FLAG	Emiliani et al., 1998	pcDNA3.1	human	
HDAC1-GFP	kind gift from J Steve	eGFP-C3	human	
HDAC2-MYC	kind gift of Tony Kouzarides lab	pcDNA3.1/myc-HisA	mouse	evex 305
HDAC3-MYC	kind gift of Tony Kouzarides lab	pCMV3-Amyc	human	evex 476
His3.3-Snap	kind gift of Dr. S. Polo. (University Paris-Diderot, France)	pSNAPf	human	NEB (N9183)
HSF2alpha WT and mutant-Snap	See Materials and Methods	pSNAPf	human	NEB (N9181)
HSF2alpha-CTAP(GS)-Gw	Bürckstümmer et al., 2006	PCEMM-CTAP	mouse	Euroscarf
HSF2alpha-Myc	Alastalo et al., 2003	pcDNA4™/TO/myc-His-A	human	Life Technologie
HSF2beta-CTAP(GS)-Gw	Bürckstümmer et al., 2006	PCEMM-CTAP	mouse	Euroscarf
HSF2beta-Flag	Pirkkala et al., 2000	pFLAG-CMV-2	mouse	Sigma-Aldrich
HSF2beta-Flag deletion mutants	Alastalo et al., 2003	pFLAG-CMV-2	mouse	Sigma-Aldrich
HSF2beta-YFP	cf materials and methods	pEYFP-C1	mouse	Clontech
Kix WT-GST	kind gift from Dr. Lemassson; Yan et al., 1998	pGEX-2T	mouse	
Kix YAY-GST	kind gift from Dr. Lemassson; Cook et al., 2011	pGEX-2T	mouse	
Myc tag		pcDNA3.1 MycHis		Life technology (V80020)

The human HSF2-Snap (WT/mutants) were constructed from the HSF2-Myc (WT/mutants) plasmid after digestion of the inserts by EcoRI and KpnI and cloning into the EcoRI and EcoRV sites in frame with the C-terminal Flag tag in pSNAPf plasmid using In-Fusion Kit (Clontech). The human HSF2-YFP was constructed by PCR and cloned into the XhoI and SalI sites in frame with the N-terminal YFP tag in EGFp-C1 plasmid using In-Fusion Kit (Clontech). All PCR-amplified products for both plasmids were sequenced to exclude the possibility of second site mutagenesis. The cDNA coding for the acetyltransferase domain of murine CBP (1097-1774) was a kind gift of Pr. Ricardo Dalla-Favera (Columbia University, New York) and was used to generate cDNA coding for key domains of CBP: Full HAT (1096-1700), HAT (1322-1700), RING (1205-1279), PHD (1280-1321), Bromodomain (1096-1205), later sub-cloned in pet28a plasmid (Invitrogen) in order to produce 6 His-tagged proteins.

Patient material

Informed consent for skin biopsy and culture of PSFs were obtained from the RSTS patients'parents (Patients 1 and 2, [P1] AND [P2]; CHU, Robert Debré Hospital, Paris, France ; Drs S ; Passemard and A. Verloes), in accordance with the Declaration of Helsinki and approved by the local ethics committee, CPP Ile de France, agreement n° P10012 8. PSFs from healthy donors have been described in Yehezkel et al., 2008). PSFs were grown in HAM's F10 supplemented with 12% FBS in humidified atmosphere with 5 % CO2 at 37°C. See Figure S7A for a description of the deletion or mutation carried by the patients.

Cell lines

Cell culture, transfections and treatments: Murine N2A (N2A, DSMZ # ACC 148), Hamster BHK, Human fibroblasts (HD), HEK293T (ATCC®, CRL-11268™), U2OS (osteosarcoma, ATCC®, HTB-96™), U2OS-Crispr*HSF2*KO (2KO), BHK cells (kindly provided by Dr.Leonhardt H and cultured as described (Herce et *al.*, 2013) and HeLa-S3 (kindly provided by Dr. Slimane Ait-Si-Ali and cultured as described (Yahi *et al.*, 2008)) cells were grown in DMEM (Lonza Group Ltd.) supplemented with 4,5 g/L glucose and 10% fetal bovine serum (FBS, Life technology) in humidified atmosphere with 5 % CO2 at 37°C. RSTS lymphoblastoid cells were obtained from Dr. D Lacombe (CHU Bordeaux; patient 3 (P3)) and from CRB-Institut Médical Jérôme Lejeune, CRB-BioJeL (BB-0033-00016; May 05, 2018, Paris; patients 4 and 5 (P4 and P5)). Lymphoblastoid cells were grown in RPMI (Life technology) supplemented with 4,5 g/L glucose and 10% FBS with L-glutamine (Life technology) in humidified atmosphere with 5 %

bioRxiv preprint doi: https://doi.org/10.1101/481457; this version posted December 26, 2018. The copyright holder for this preprint (which was not certified by peer review) is the author/funder. All rights reserved. No reuse allowed without permission.

CO2 at 37°C. See Figure S7A for a description of the deletion or mutation carried by the patients.

Mice model

Specific pathogen-free C57BL/N female mice were purchased from Janvier (Lyon, France) and maintained in sterile housing in accordance with the guidelines of the Ministère de la Recherche et de la Technologie (Paris, France). Rodent laboratory food and water were provided ad libitum. Experiments were performed in accordance with French and European guidelines for the care and use of laboratory animals. The project has been approved by the Animal Experimentation Ethical Committee Buffon (CEEA-40) and recorded under the following reference with the Ministère de l'Enseignement Supérieur et de la Recherche (#2016040414515579).

Patients' primary fibroblasts

For fibroblasts primary cells, The study was conducted in accordance with the Declaration of Helsinki with an approved written consent form for each patient (CPP ESTI: 2014/39 ; N°ID: 2014-A00968-39), and approval was obtained from the local ethics committee ESTI (license: NCT02873832).

Generation of CRISPR/Cas9 *Hsf2*KO U2OS cells

Guide RNAs (gRNA) targeting the exon 1 of *HSF2* were designed using our own software (http://crispor.tefor.net/) and cloned into pMLM3636 guide RNA expression plasmid (Addgene 43860). U2OS cells were transfected with Cas9 and guide RNA expression plasmids using Amaxa electroporation as recommended by the manufacturer (Lonza). Cas9 expression plasmid was from the Church lab (Addgene 41815). One week after transfections, cells were seeded at single cell density. Clones were genotyped by DNA sequencing of PCR products spanning the targeted region of the *HSF2* gene. The selected U2OS clone presented 3 different outframe mutations on *HSF2* exon 1, each corresponding to a different allele (Supplementary Table 2). Guide RNA sequence targeting the 1st AUG on *HSF2* exon 1: 5′-UGCGCCGCGUUAACAAUGAA-3′. Primers used for PCR cloning for validation: forward (hHSF2_Cr_ATG_F): 5′-AGTCGGCTCCTGGGATTG-3′ and reverse (hHSF2_Cr_ATG_R): 5′-AGTGAGGAGGCGGTTATTCAG-3′. The genomic sequences of the mutated h*HSF2* alleles and the resulting lack in HSF2 protein and HSF2 DNA-binding activity are described in Table in Figure S5B. The selected U2OS clone presented 3 different out-frame mutations in the *HSF2* exon1, each one corresponding to a different allele (see Figure S5B).

Production of KIX-GST, His-CBP domain and HSF2 proteins

Escherichia coli 21 (DE3) were transformed with the different 6His-tag CBP constructs for production of the different CBP domains as previously described (Duval et al, 2015). All proteins were stored in 20 mM Tris-HCl, 150 mM NaCl, pH 7.5 and kept at -80°C until use. *E. coli* BL21 bacteria were transformed with the different GST-KIX constructs (Cook et al., 2011) and grown in presence of ampicilline and chloramphenicol at 37°C (4-6h). Bacteria were then grown with 1 mM Isopropyl β-D-1-thiogalactopyranoside over-night. After centrifugation (4400 rpm at 4°C), bacteria were lysed in PBS pH8, 300mM NaCl, Triton X100 1%, 1mg/mL lysozyme, protease inhibitors under stirring at 4°C for 30min. Bacteria were sonicated (BRANSON sonicator, power 20%, 10'' ON/20''OFF) and centrifugated at 4°C, 16000g for 30 min. Gluthatione sepharose 4B beads (G4510-10ML Sigma-Aldrich) were added to the cleared supernatants and subjected to rotation for 1h30 min at 4°C. The mixture was loaded into a column (Sigma-Aldrich) and washed with PBS/NaCl 300mM pH8, then Tris 50 mM/NaCl 150 mM pH8. Proteins were eluted with 5mL of elution buffer (50mM Tris HCl pH8, 150 mM NaCl, 10 mM GSH). The protein concentration was measured using Bradford method. *In vitro* transcription and translation reactions were performed using a TNT T7 coupled reticulocyte lysate system as recommended by the supplier (Promega, Charbonnieres-les-Bains, France). 1 µg of the plasmid DNA template was transcribed and the protein was translated at 30°C for 90 min.

Immunoprecipitation and Western blotting

bioRxiv preprint doi: https://doi.org/10.1101/481457; this version posted December 26, 2018. The copyright holder for this preprint (which was not certified by peer review) is the author/funder. All rights reserved. No reuse allowed without permission.

Protein extracts from cells were prepared using a modified Laemmli buffer (5% sodium dodecyl sulphate, 10 % glycerol, 32.9 mM Tris-HCl pH 6.8) supplemented with protease inhibitors (Sigma-Aldrich). Brain tissues were prepared with a lysis buffer (Hepes 10 mM ph 7,9; NaCl 0.4M, EGTA 0.1 M; glycerol 5 %, DTT 1 mM, PMSF 1 mM, protease inhibitor (Sigma-Aldrich), phosphatase inhibitor (Roche)). Then, 30 µg of proteins from lysates were subjected to migration on 8–12% acrylamide gels and transferred on to polyvinylidene difluoride membranes (GE Healthcare Europe GmbH) in borate buffer (50 mM Tris-HCl and 50 mM borate) for 1h45 at constant voltage (48 V). The membranes were incubated with primary antibodies overnight at 4 °C, then washed in Tris-buffered saline–Tween 0.1% and incubated for 1 h with horseradish peroxidase (HRP)-coupled secondary antibody (Jackson Immunoresearch). The signal was revealed using a chemiluminescent reagent (Pierce® ECL Plus Western Blotting Substrate, Thermo Scientific) and was detected using hyperfilm (HyperfilmTM ECL, Amersham Biosciences) and a film processor (Konica Minolta). Poly-ubiquitinated HSF2 was detected as described in Ahlskog et al., 2010.

Biolayer Interferometry

For *in vitro* protein-protein interaction experiments, we used biolayer interferometry technology (Octet Red, Forté-Bio,USA). Recombinant HSF2 (TP310751 Origen) was desalted (ZebaTM Spin Desalting Columns, 7K molecular-weight cutoff, 0.5 ml (1034–1164, Fisher Scientific, Germany)) and biotinylated at a molar ratio biotin/protein (3:1) for 30 min at room temperature (EZ-Link NHS-PEG4-Biotin (1189-1195, Fisher Scientific, Germany)). Excess Biotin was removed using ZebaTM Spin Desalting Columns. Biotinylated recombinant HSF2 was used as a ligand and immobilized at 100 nM on streptavidin biosensors after dilution in phosphate-buffered saline (PBS; 600s). Interactions with desalted analytes diluted in PBS at 100 nM (recombinant CBP domains 6His-tag Full HAT, Bromodomain (BD), RING), or HSP70 as a positive control (ADI-SPP-555, Enzo- Life Sciences)) were analysed after association (600 s). All sensorgrams were corrected for baseline drift by subtracting a control sensor exposed to running buffer only.

<u>For immunoprecipitation of exogenous proteins, using GFP-Trap</u>. GFP-Trap®-A (ChromoTek) contains a small recombinant fragment of alpaca anti-GFP-antibody, covalently coupled to the surface of agarose beads. It enables purification of any protein of interest fused to GFP, eGFP, YFP, CFP or Venus. HEK 293 cells were transfected by a combination YFP- or Myc-tagged hHSF2 and HA-tagged EP300, CBP (WT or DN) or GFP-tagged HDAC1, or mock vector, with XtremGENE HP Reagent (Sigma-Aldrich) following manufacturer's instructions. Cells were lysed in Lysis buffer (50 mM Hepes pH 8, 100 mM NaCl, 5 mM EDTA, Triton X-100 0.5 %, Glycerol 10 %, VPA (1 mM), DTT 1 mM, PMSF 1 mM, proteases inhibitors, phosphatase inhibitors (Roche)) and then, HSF2 was immunoprecipitated using anti-GFP-trap antibody. Immunoprecipitated proteins were run on a 8 % SDS-polyacrylamide gel, followed by an immunodetection of CBP or EP300 protein using anti-HA antibody. The amount of immunoprecipitated HSF2 was determined after reblot of the IP membrane with an anti-GFP or anti-Myc antibody. The amount of HSF2 and CBP or EP300 proteins, in the input samples, were detected with anti-GFP or Myc and anti-HA antibodies, respectively.

<u>For immunoprecipitation of endogenous proteins</u>. Brain cortices or organoids, or cells (SHSY5Y, N2a) were lysed 30min in Lysis buffer A (25 mM Hepes pH 8, 100 mM NaCl, 5 mM EDTA, Triton X-100 0,5%, VPA (1 mM), PMSF 1 mM, proteases inhibitors, phosphatase inhibitors (Roche)). After centrifugation (15 min, 12 000 g) and preclearing, cell lysates were subjected to immunoprecipitation overnight using an anti-mouse HSF2 (Santa-Cruz) and a non relevant IgG (Sigma-aldrich) as a negative control that were pre-incubated 1h at RT with Protein G UltraLink Resin beads (53132, Pierce). Protein complexes were then washed 4 times in wash buffer (25 mM Tris HCl pH 7.5, 150 mM NaCl, 1 mM EDTA, Triton X-100 0.1 % Glycerol 10 %, 1 mM VPA, 1 mM PMSF, proteases inhibitors, phosphatase inhibitors (Roche)), and suspended in 2x Laemmli buffer. After boiling, the immunoprecipitates were resolved in 8 % SDS-PAGE and immunoblots were performed using an anti-rabbit pan acetyl-Lysine, anti-mouse HSF2 (Santa-Cruz), EP300 (Santa-Cruz) and CBP (CST). The

bioRxiv preprint doi: https://doi.org/10.1101/481457; this version posted December 26, 2018. The copyright holder for this preprint (which was not certified by peer review) is the author/funder. All rights reserved. No reuse allowed without permission.

amount of HSF2 and CBP or EP300 proteins in the input samples were detected with anti-mouse HSF2 and anti-rabbit CBP (CST) or EP300 (Santa-Cruz) antibodies.

Purification of HSF2 from HEK293 cells and mass spectrometry analysis of acetylated lysines

The protocole used is the same as for HSF1, as described by Westerheide et al., 2009. HEK 293 cells were transfected with mouse HSF2-beta Flag with or without CMV-EP300, treated with trichostatin A or nicotinamide as indicated 18 hours prior harvesting and lysed in RIPA buffer. HSF2-Flag was immunoprecipitated using α-Flag M2 affinity gel beads (Sigma F2426) and eluted with Flag peptide. Purified mHSF2-Flag was separated by SDS-PAGE, excised from the gel, digested with trypsin, and subjected to tandem mass spectrometric analysis by a hybrid quadrupole time-of-flight instrument (QSTAR, Applied Biosystems, Foster City, CA) equipped with a nanoelectrospray source. MS/MS spectra were searched against the IPI mouse sequence database (68,222 entries; version 3.15) using Mascot (Matrix Science, Boston, MA; version 1.9.05) and X! Tandem (www.thegpm.org; version 2006.04.01.2) database 4 search algorithms. Mascot and X! Tandem were searched with a fragment and precursor ion mass tolerance of 0.3 Da assuming the digestion enzyme trypsin with the possibility of one missed cleavage. Carbamidomethylation of cysteine was included as a fixed modification whereas methionine oxidation, N-terminal protein and lysine acetylation were included as variable modifications in the database search. Peptide identifications were accepted at greater than 95.0% probability as determined by the Peptide Prophet algorithm (7) and validated by manual inspection of the MS/MS spectra, as shown in Table S2. Related to Figure 2C and S2A and Table 1.

Tandem Affinity Purification (TAP) and M/S identification of HSF2 partners in HeLa cells

We performed retroviral transduction to establish HeLa-S3 cell lines expressing double-tagged HSF2 proteins. *Hsf2*-alpha and *Hsf2*-beta cDNA, cloned from E16 mouse brain were inserted in vector PCEMM-CTAP (Euroscarf P30536; Bürckstümmer et al., 2006) with CMV-driven expression of insert and GFP used as an indirect reporter (IRES; Fig S6A). PCEMM-CTAP allows sequential immunoprecipitation of the tagged protein through two tags: protein G (able to bind IgG) and the streptavidin-binding peptide (GS-TAP; Fig S6A). These two tag-modules are separated by two clivage sites for the Tobacco Etch virus (TEV) protease. Retrovirus production (*Moloney murine leukemia* virus type) and cell transduction with CTAP-empty (no insert), CTAP- Hsf2alpha and CTAP-Hsf2beta were performed as described (Sandrin and Cosset, 2006). GFP-positive Hela-S3 clones were then isolated by clonal dilution, selected by FACS (INFLUX 500, BD BioSciences, IMAGOSEINE Platform, Jacques Monod Institute, Paris) and amplified. By FACS we could isolate four cell sub-populations according to the intensity of the GFP signal to identify a population of cells expressing the recombinant tagged protein at levels similar to that of the endogenous HSF2 protein. GFP-positive Hela-S3 clones stably expressing GS-HSF2alpha, GS-HSF2beta or empty vector, were grown in floating cultures (spinners) and 10 G of cells (3 x 10^9 cells) per cell line was collected as described (Fristch et al. 2010). Nuclear extracts were prepared as described (Fristch et al. 2010; except the DNase 1 treatment was omitted). Total nuclear extracts were incubated with IgG-agarose beads overnight (Sigma; A2909). Then beads were incubated twice with TEV enzyme (Invitrogen, ref. 12575023)) for 45 minutes transferred to Poly-prep columns (Bio-rad). Eluates were collected in TEV buffer. These eluates were then incubated with Dynabeads My-one streptavidin for 1 h, washed once, and eluted using 5 mM D-biotin. Proteins were concentrated using TCA/acetone precipitation and dissolved in Laemmli sample buffer. Samples from three independent experiments were sequentially sent to TAPLIN Biological Mass Spectrometry Facility (Harvard Medical School, Boston, MA, USA) for MS (LC/MS/MS) analysis as in Fristch et al. (2010).

Immunoprecipitation and MS analysis of the endogenous HSF2 protein from E17 mouse cortices

We also analyzed by MS the partners of the endogenous protein HSF2 from E17 fetal cortices. Brain cortices were mechanically lysed into 4.5 volumes of the following buffer: 10 mM Hepes (pH 7.9), 400 mM NaCl, 5 %, glycerol, 100 mM EGTA) and two cycles of freezing and thawing in liquid nitrogen, and centrifuged at 20,000 g for 30 min. Supernatants were used to immunoprecipitate HSF2 using a

bioRxiv preprint doi: https://doi.org/10.1101/481457; this version posted December 26, 2018. The copyright holder for this preprint (which was not certified by peer review) is the author/funder. All rights reserved. No reuse allowed without permission.

monoclonal antibody (Abcam) or PBS as a negative control, and protein G agarose (Roche). Immunoprecipitates were analyzed on SDS-PAGE gel bands, containing the HSF2 protein (staining with colloidal blue) were sent to TAPLIN Biological Mass Spectrometry Facility (Harvard Medical School, Boston, MA, USA) for MS (LC/MS/MS) analysis.

SNAP-Tag labelling of HSF2 molecules and analysis of protein decay

CRISPR/Cas9 *Hsf2*KO U2OS cells were transfected with SNAP-tagged- HSF2 WT, -HSF2 3KQ or -HSF2 3KR constructs (Xtrem-Gen HP, Sigma-Aldrich), incubated in the presence of the cell-permeable SNAP-Cell® Oregon green fluorescent substrate (1,25 mM) and then with SNAP-Cell® Block (0,5mM) during the pulse chase according to the manufacturer's instructions (New England Biolabs). Cells were lysed in modified Laemmli buffer (5 % SDS, 10% glycerol, 32.9 mM Tris-HCl pH 6.8) supplemented with 1 mM DTT (Sigma-Aldrich), and their extracts (15 µG) run on precast 4-20% Mini-Protean TGX gel (BioRad) and run as for western blots. Gels were scanned on a Typhoon Trio imager (GE Healthcare; excitation 532 nm, emission 580 nm, PMT 700 V) for determination of signal intensity of the covalently-bound fluorescent products as described in (Sanial et al., 2017).

Fluorescence three-hybrid assay

Fluorescence three-hybrid assay was performed according to Herce *et al.* (2013). BHK cells were transfected with constructs expressing expressing YFP-HSF2, CBP-HA, or EP300-HA, and GBP-LacI, using different combinations (ratio 1:1.5:2) at 70-80 % confluency using reverse transfection by Lipofectamine 2000 (ThermoFisher Scientific), as indicated. Medium was changed after 4 hours for all transfection. After 24 h, the cells were fixed in 4 % paraformaldehyde on coverslip and stained with mouse anti-HA (Covance) or rabbit anti-CBP antibody (Santa-Cruz), followed by a staining with mouse or rabbit Cy3 secondary antibody (Jackson Immunoresearch), respectively. Confocal microscopy images were taken on a confocal microscope Leica TCS SP5 (IMAGOSEINE Imaging Platform in Institut Jacques Monod) and images were analyzed using Fiji software.

Modeling of the HR-A/B domain and KIX domain of CBP

Prediction of secondary structure of the HSF2 HR-A/B domain was performed using Psipred (http://bioinf.cs.ucl.ac.uk/psipred/) and nps@ (https://npsa-prabi.ibcp.fr/). The tertiary structure of the same domain was predicted using http://petitjeanmichel.free.fr/itoweb.petitjean.freeware.html. Sequence similarity between human HSF2 HR-A/B (Sandqvist et al., 2009), lipoprotein Lpp56 of *E. coli* (Shu et al., 2000), yeast transcriptional factor GCN4 (mutated on some residues to stabilize heptad repeats; Shu et al., 1999) and murine PTRF (Polymerase I and Transcript-Release Factor) and human ATF2 (Activating Transcription Factor 2; a member of the ATF/CREB family) that is known to interact with CBP/EP300 (*Bordoli et al., 2001*) was explored using *Uniprot* (Pundir et al., 2017*;* https://www.uniprot.org/) and *ClustalW* (Thompson et al., 1994*;* https://www.ebi.ac.uk/Tools/msa/clustalw2/). Step 1: Based on this sequence similarity a sequence alignment of HR-A/B was developed (using *Uniprot and ClustalW*; see Figure S3C), a structural model of the monomer HR-A/B was generated using using *Modeller* (v9.19 (Eswar et al., 2006*;* https://salilab.org/modeller/), verified by *ERRAT* (Colovos et al., 1993*;* http://servicesn.mbi.ucla.edu/ERRAT/) and *RESprox* (Berjanskii et al., 2012*;* http://www.resprox.ca/) and ramachandran plot (Ramachandran et al., 1963) followed by the development of the trimer using *SymmDock* (Schneidman-Duhovny *et al.*, 2005 ; v Beta 1.0; http://bioinfo3d.cs.tau.ac.il/SymmDock/). Step 2: the interaction between HR-A/B and the KIX domain (pdb: 2LXT; Brüschweiler et al., 2013) was simulated and compared using *Zdock* (v 2.1; Pierce et *al.*, 2014) and *Firedock* (Mashiach et al., 2008; Odoux et al., 2016). More precisely, the ten best results generated by *Zdock* and *Firedock*, and scored according to their Root Mean Square Deviation (RMSD), which were compared thanks to a visualization program ICM (Fernandez-Recio et al, 2005). The mutation of the key residuse involved in the interaction between HR-A/B and the KIX domain have been performed using PyMOL (v2.0) and the docking was done as described above.

bioRxiv preprint doi: https://doi.org/10.1101/481457; this version posted December 26, 2018. The copyright holder for this preprint (which was not certified by peer review) is the author/funder. All rights reserved. No reuse allowed without permission.

RP-UFLC-based separation and quantification of CBP substrate peptides (HSF2) and their acetylated forms

For acetylation assays, we synthetized several 5-fluorescein amidite (5-FAM)-conjugated peptide substrates based on the human HSF2 sequence and containing various lysine residues of interest (Proteogenix):

- 5-FAM-SGIVK82QERD-NH2, referred to as K82 peptide
- 5-FAM-SSAQ135VQIR-NH2, referred to as K135 peptide
- 5-FAM-SLRRK197RPLL-NH2, referred to as K197 peptide

NB: the synthesis of the HSF2 K128 peptide failed repeatedly because of its insolubility (Manufacturer's information).

We also synthesized acetylated versions of these HSF2 peptides as standards. Samples containing HSF2 peptides and their acetylated forms were separated by RP-UFLC (Shimadzu) using Shim-pack XR-ODS column 2.0 x 100 mm 12 nm pores at 40°C. The mobile phase used for the separation consisted of 2 solvents: A was water with 0.12 % trifluoacetic acid (TFA) and B was acetonitrile with 0.12 % TFA. Separation was performed by an isocratic flow depending on the peptide:

- 80 % A/20 % B, rate of 1 ml/min for K82 and K135
- 77 % A/23 % B, rate of 1 ml/min for K195 and K197

HSF2 peptide (substrate) and their acetylated forms (products) were monitored by fluorescence emission (λ= 530 nm) after excitation at λ= 485 nm and quantified by integration of the peak absorbance area, employing a calibration curve established with various known concentrations of peptides.

***In vitro* acetyltransferase assay**

To determine the activity of recombinant CBP-Full HAT on HSF2 peptides, we used 96-wells ELISA plate (Thermofisher) and assays were performed in a total volume of 50 µL of acetyltransferase buffer (50 mM Tris pH8, 50 mM NaCl) with 500 nm CBP-Full HAT, 50 µM HSF2 peptides and 1 mM dithiothreitol (DTT). Reaction was then started with the addition of 100 µM Acetyl-CoA (AcCoA) and the mixture was incubated 20 min at room temperature. 50 µL of $HClO_4$ (15 % in water, v/v) was used to stop the reaction and 10 µL of the mixture were injected into the RP-UFLC column for analysis. For time course studies, aliquots of the mother solution were collected at different time points and quenched with 50 µL of $HClO_4$ prior to RP-UFLC analysis.

bioRxiv preprint doi: https://doi.org/10.1101/481457; this version posted December 26, 2018. The copyright holder for this preprint (which was not certified by peer review) is the author/funder. All rights reserved. No reuse allowed without permission.

SUPPLEMENTAL EXPERIMENTAL PROCEDURE

Related to Figure S3A:

For *in vitro* protein-protein interaction experiments, we used biolayer interferometry technology (Octet Red, Forté-Bio). Recombinant HSF2 (TP310751 Origen) was desalted (ZebaTM Spin Desalting Columns, 7K molecular-weight cutoff, 0.5 ml (1034–1164, Fisher Scientific Germany)) and biotinylated at a molar ratio biotin/protein (3:1) for 30 min at room temperature (EZ-Link NHS-PEG4-Biotin (1189-1195, Fisher Scientific Germany)). Excess Biotin was removed using ZebaTM Spin Desalting Columns. Biotinylated recombinant HSF2 was used as a ligand and immobilized at 100 nM on streptavidin biosensors after dilution in phosphate-buffered saline (PBS; 600 s). Interactions with desalted analytes diluted in PBS at 100 nM (recombinant CBP domains 6His tag (Full HAT) or HSP70 as a positive control (ADI-SPP-555, Enzo- Life Sciences)) were analysed after association (600 s) and dissociation (600 s) steps at 26 °C. All sensorgrams were corrected for baseline drift by subtracting a control sensor exposed to running buffer only. Each KD was determined with a 1:1 stoichiometry model using a global fit with Rmax unlinked by sensor (FortéBio, Data analysis software version 7.1.0.89).

	Sequence	Mutations	Protein product
WT	TGCGCCGCGTTAACAATGAAGCAGAGTTCGAACGTGCCGGCTT TCCTCAGCAAGCTGTGGACGCTTGTGGAGGAAACCCACACTAA CGAGTTCATCACCT		HSF WT protein
Allele 1	TGCGCCGCGTTAACAATGAAG~~C~~AGAGTTCGAACGTGCCGGCTT TCCTCAGCAAGCTGTGGACGCTTGTGGAGGAAACCCACACTAA CGAGTTCATCACCT	1nt deletion	A 61aa truncated protein (only the 1st 6 aa are identical to HSF2)
Allele 2	TGCGCCGCGTTAACAATGAAGCAGAGTTCGAAC~~G~~TGCCGGCTT **C**CCTCAGCAAGCTGTGGACGCTTGTGGAGGAAACCCACACTAA CGAGTTCATCACCT	1nt deletion + 1 substitution	A 61aa truncated protein (only the 1st 6 aa are identical to HSF2)
Allele 3	TGCGCCGCGTTAACAATGAAGCAGAGTTCGAACG~~TGCCGGCTT TCCTCAGCAAG~~CTGTGGACGCTTGTGGAGGAAACCCACACTAA CGAGTTCATCACCT	20nt deletion	A 16aa truncated protein (only the 1st 5 aa are identical to HSF2)

bioRxiv preprint doi: https://doi.org/10.1101/481457; this version posted December 26, 2018. The copyright holder for this preprint (which was not certified by peer review) is the author/funder. All rights reserved. No reuse allowed without permission.

LIST OF SUPPLEMENTARY FIGURES

Supplemental Information includes ten figures. Figure S1 to S7 are relative to Figure 1 to 7.

LIST OF TABLES

Table 1. Summary of the HSF2 acetylated peptides identified by MS
Table 2. Original tables and spectra corresponding to the HSF2 acetylated peptides identified by MS

bioRxiv preprint doi: https://doi.org/10.1101/481457; this version posted December 26, 2018. The copyright holder for this preprint (which was not certified by peer review) is the author/funder. All rights reserved. No reuse allowed without permission.

Figure 1

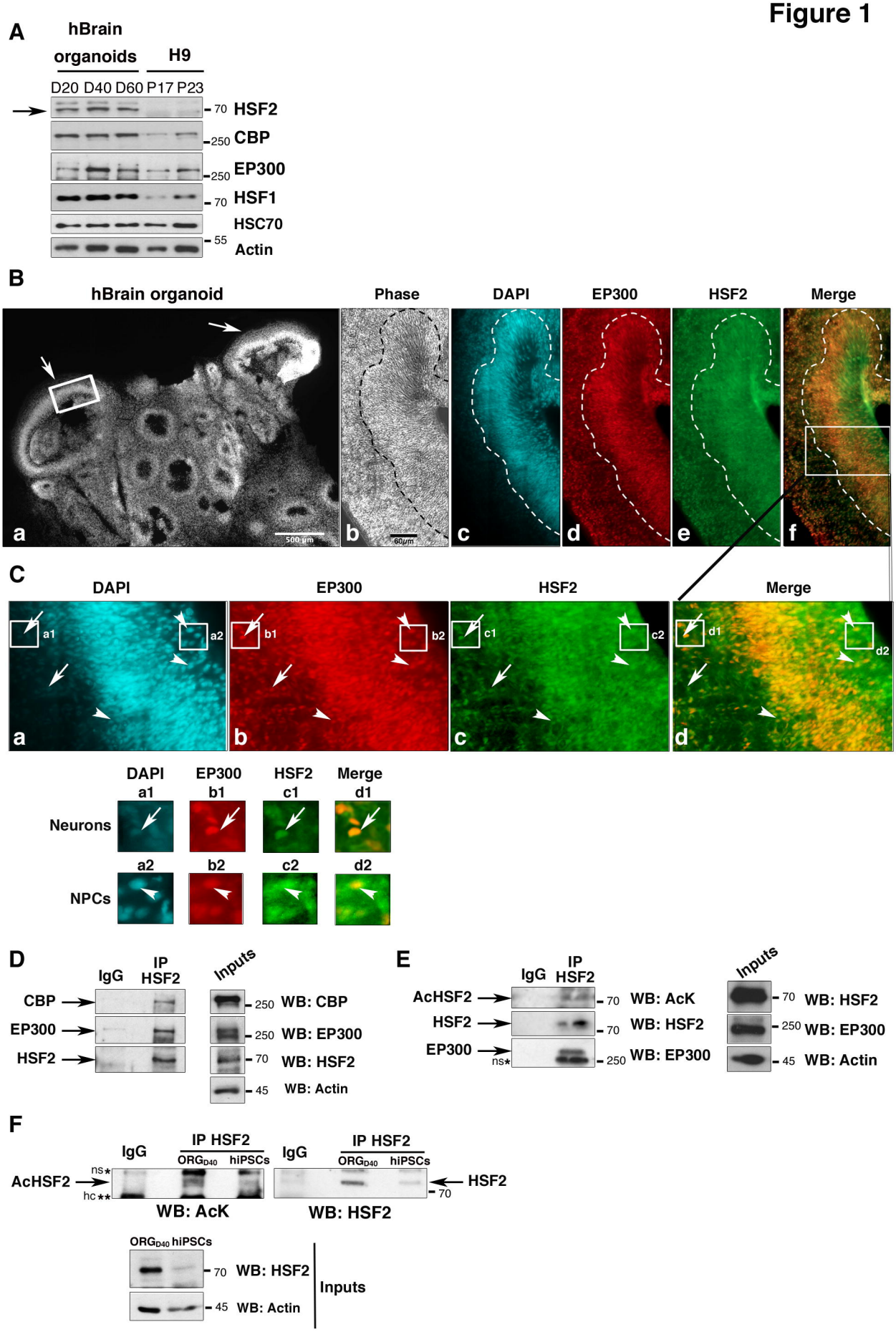

Figure 2

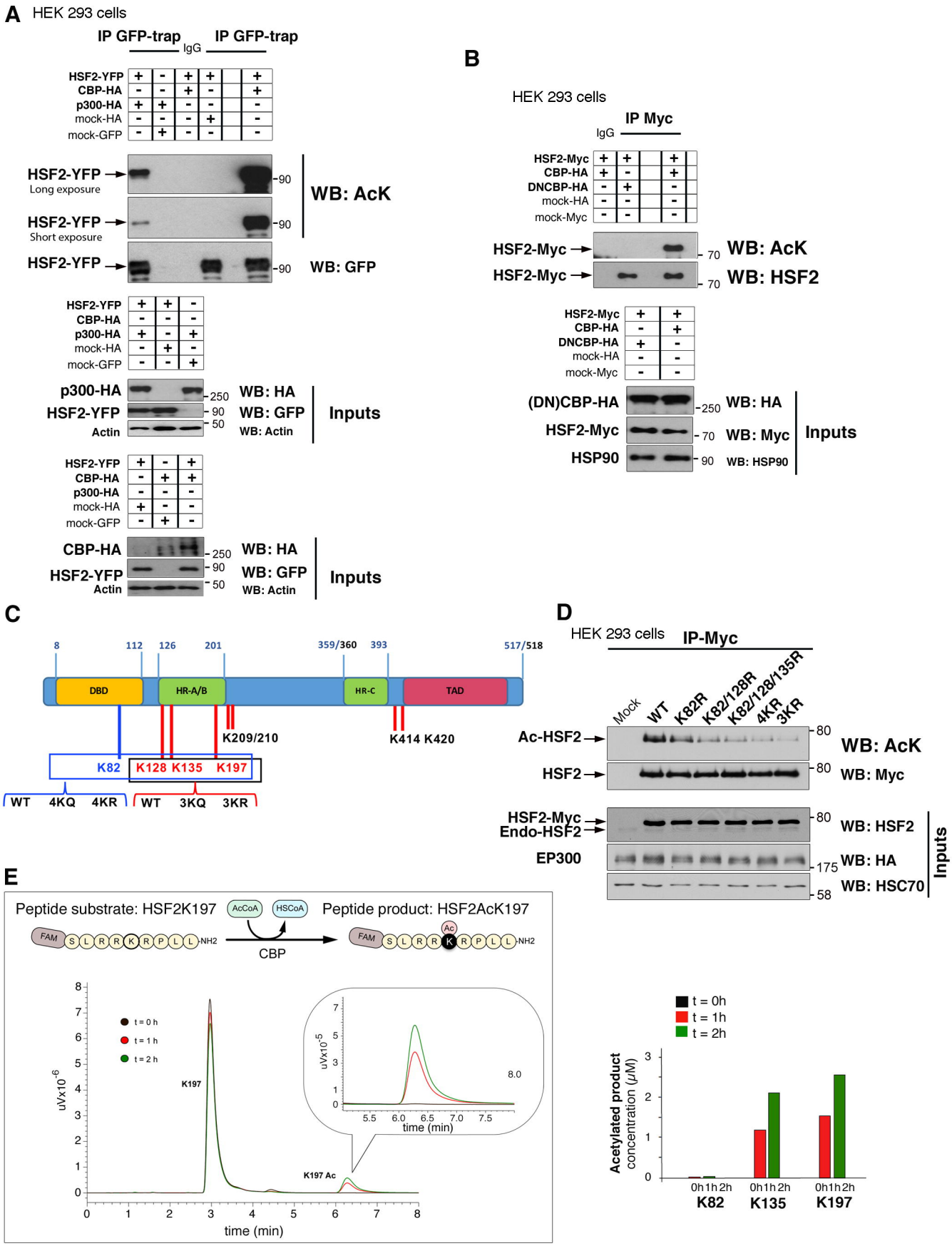
A
HEK 293 cells
IP GFP-trap
IgG
IP GFP-trap
HSF2-YFP
CBP-HA
p300-HA
mock-HA
mock-GFP
HSF2-YFP
Long exposure
HSF2-YFP
Short exposure
HSF2-YFP
WB: AcK
WB: GFP
p300-HA
HSF2-YFP
Actin
WB: HA
WB: GFP
WB: Actin
Inputs
CBP-HA
HSF2-YFP
Actin
WB: HA
WB: GFP
WB: Actin
Inputs
B
HEK 293 cells
IP Myc
IgG
HSF2-Myc
CBP-HA
DNCBP-HA
mock-HA
mock-Myc
HSF2-Myc
HSF2-Myc
WB: AcK
WB: HSF2
(DN)CBP-HA
HSF2-Myc
HSP90
WB: HA
WB: Myc
WB: HSP90
Inputs
C
8
112
126
201
359/360
393
517/518
DBD
HR-A/B
HR-C
TAD
K209/210
K414 K420
K82
K128 K135
K197
WT
4KQ
4KR
WT
3KQ
3KR
D
HEK 293 cells
IP-Myc
Mock
WT
K82R
K82/128R
K82/128/135R
4KR
3KR
Ac-HSF2
HSF2
WB: AcK
WB: Myc
HSF2-Myc
Endo-HSF2
EP300
WB: HSF2
WB: HA
WB: HSC70
Inputs
E
Peptide substrate: HSF2K197
AcCoA
HSCoA
Peptide product: HSF2AcK197
CBP
FAM
S L R R K R P L L NH2
Ac
t = 0 h
t = 1 h
t = 2 h
K197
K197 Ac
uVx10-6
uVx10-5
time (min)
8.0
t = 0h
t = 1h
t = 2h
Acetylated product concentration (μM)
0h 1h 2h
K82
K135
K197

bioRxiv preprint doi: https://doi.org/10.1101/481457; this version posted December 26, 2018. The copyright holder for this preprint (which was not certified by peer review) is the author/funder. All rights reserved. No reuse allowed without permission.

Figure 3

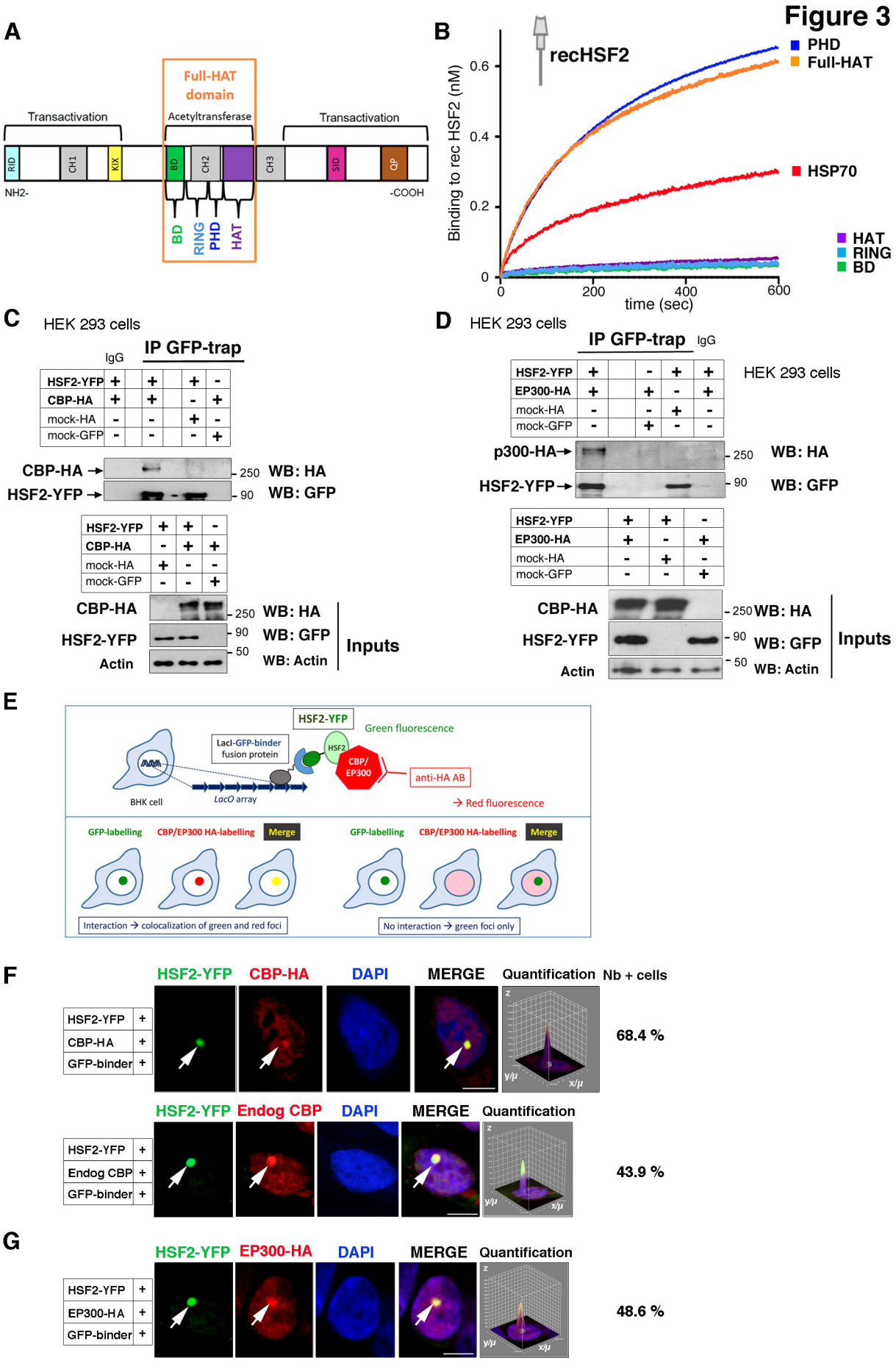

bioRxiv preprint doi: https://doi.org/10.1101/481457; this version posted December 26, 2018. The copyright holder for this preprint (which was not certified by peer review) is the author/funder. All rights reserved. No reuse allowed without permission.

Figure 4

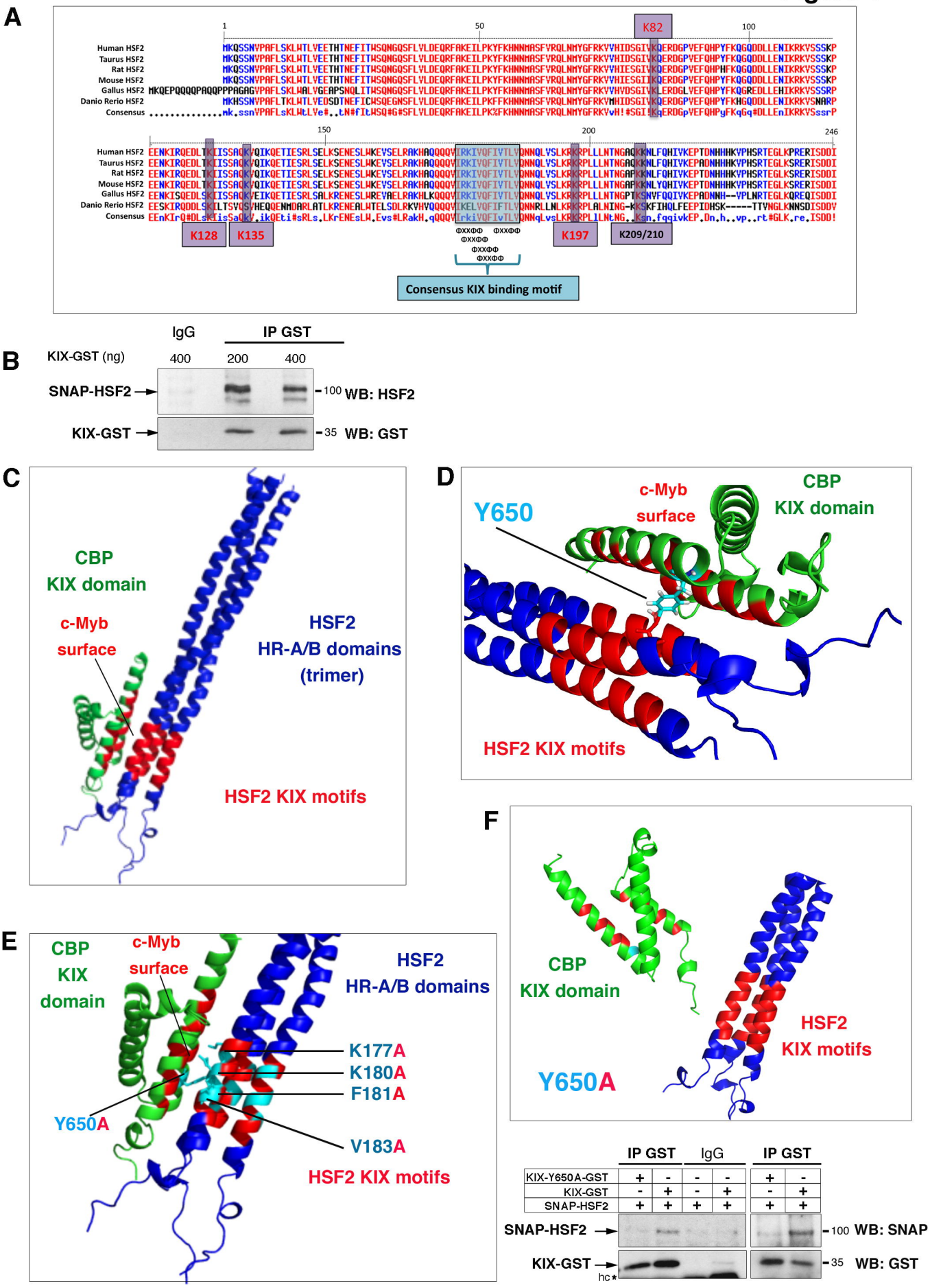

Figure 5

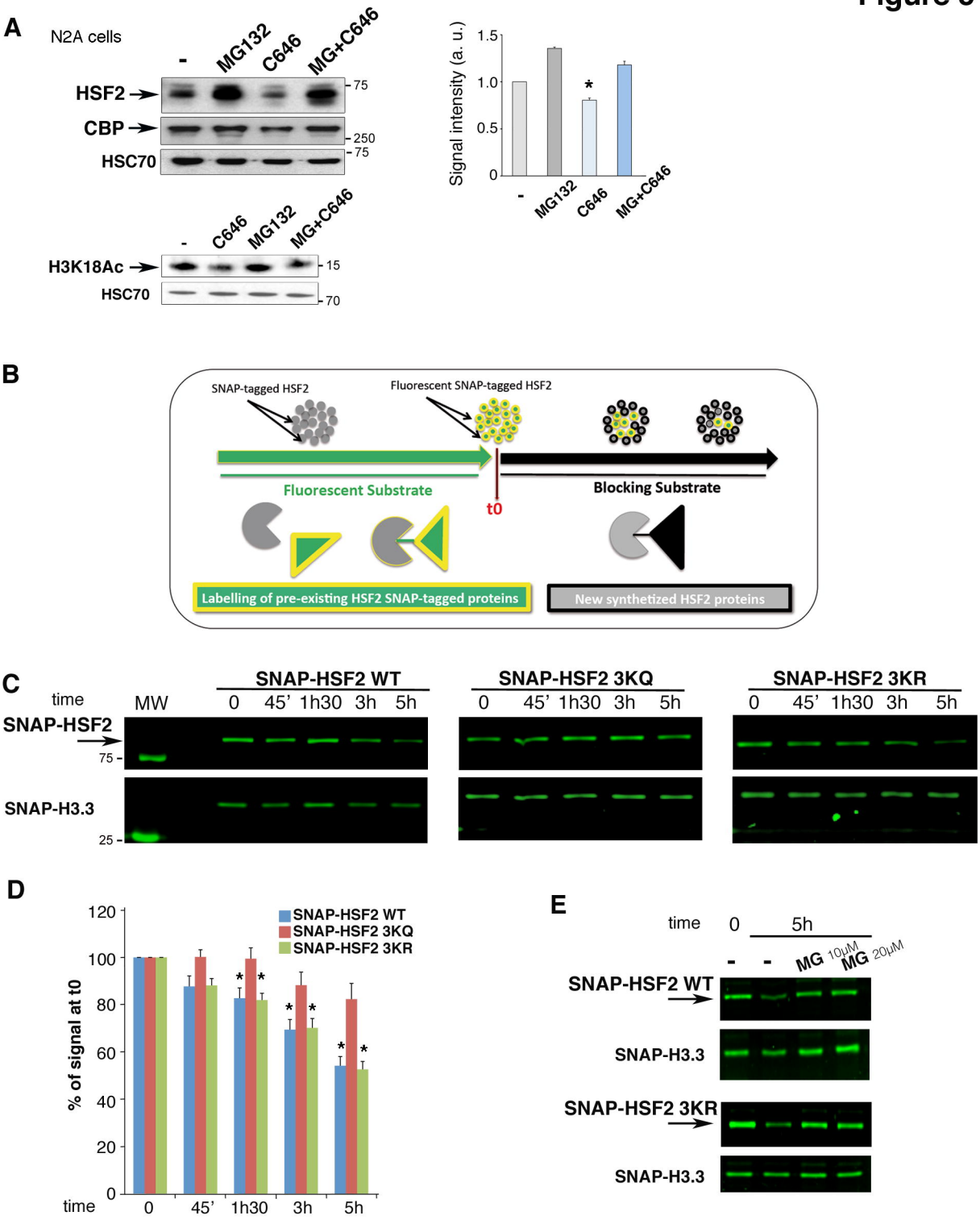
A
N2A cells
-
MG132
C646
MG+C646
HSF2
CBP
HSC70
75
250
75
Signal intensity (a. u.)
1.5
1.0
0.5
0
*
-
MG132
C646
MG+C646
-
C646
MG132
MG+C646
H3K18Ac
HSC70
15
70
B
SNAP-tagged HSF2
Fluorescent SNAP-tagged HSF2
Fluorescent Substrate
t0
Blocking Substrate
Labelling of pre-existing HSF2 SNAP-tagged proteins
New synthetized HSF2 proteins
C
time
MW
SNAP-HSF2 WT
SNAP-HSF2 3KQ
SNAP-HSF2 3KR
0
45'
1h30
3h
5h
SNAP-HSF2
75
SNAP-H3.3
25
D
% of signal at t0
120
100
80
60
40
20
0
SNAP-HSF2 WT
SNAP-HSF2 3KQ
SNAP-HSF2 3KR
time
0
45'
1h30
3h
5h
E
time
0
5h
-
-
MG 10µM
MG 20µM
SNAP-HSF2 WT
SNAP-H3.3
SNAP-HSF2 3KR
SNAP-H3.3

bioRxiv preprint doi: https://doi.org/10.1101/481457; this version posted December 26, 2018. The copyright holder for this preprint (which was not certified by peer review) is the author/funder. All rights reserved. No reuse allowed without permission.

Figure 6

A

Sample type	number of protein matches	protein match	uniprtoKB code
TAP: HSF2 alpha	2	UPSP:HSF2_HUMAN	Q03933
	1	UPSP:HDAC1_HUMAN	Q13547
	1	UPSP:NUP62_HUMAN	P37198
TAP: HSF2 beta	1	UPSP:HDAC1_HUMAN	Q13547
	1	UPSP:HSF2_HUMAN	Q03933

B

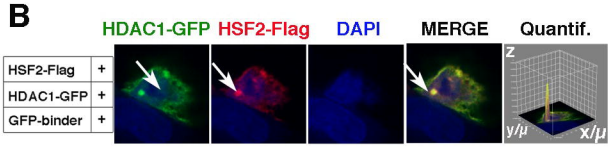

C

HEK 293 cells

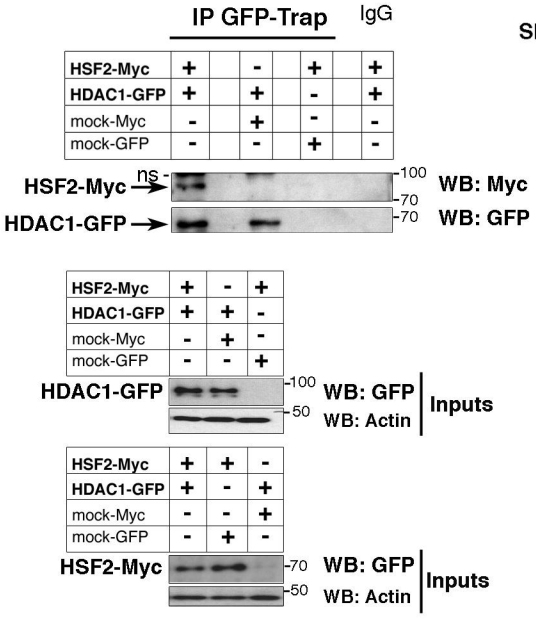

D

HEK 293 cells

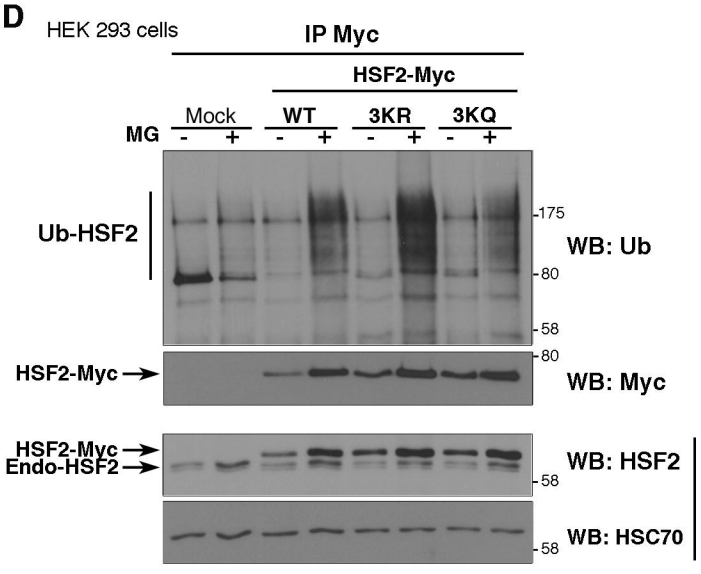

E

HEK 293 cells

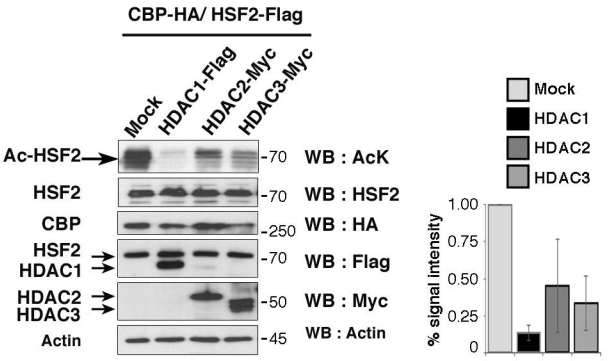

F

U2OS 2KO cells

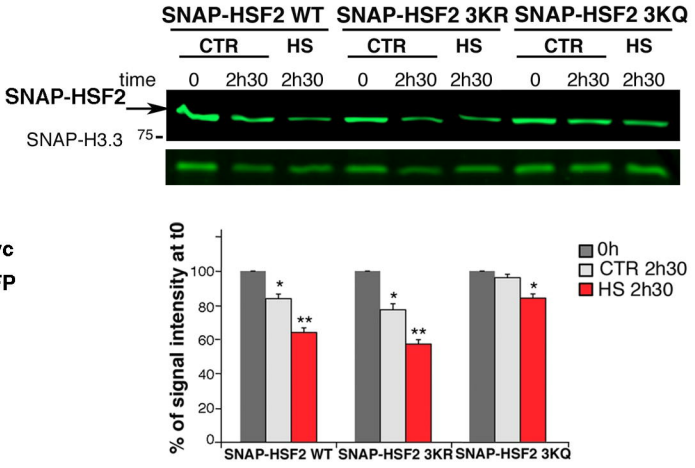

G

N2A cells

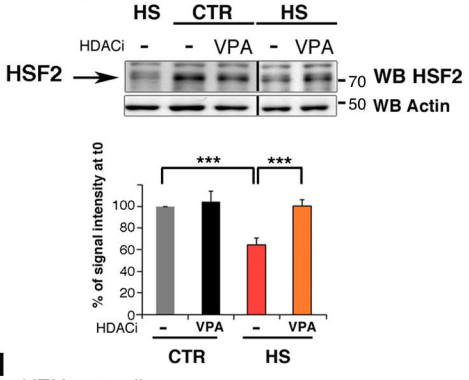

H

HEK 293 cells

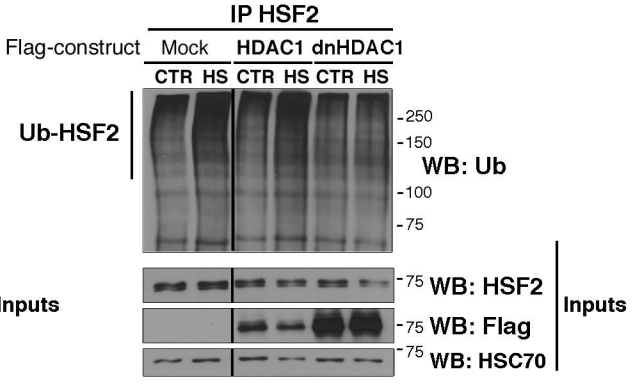

bioRxiv preprint doi: https://doi.org/10.1101/481457; this version posted December 26, 2018. The copyright holder for this preprint (which was not certified by peer review) is the author/funder. All rights reserved. No reuse allowed without permission.
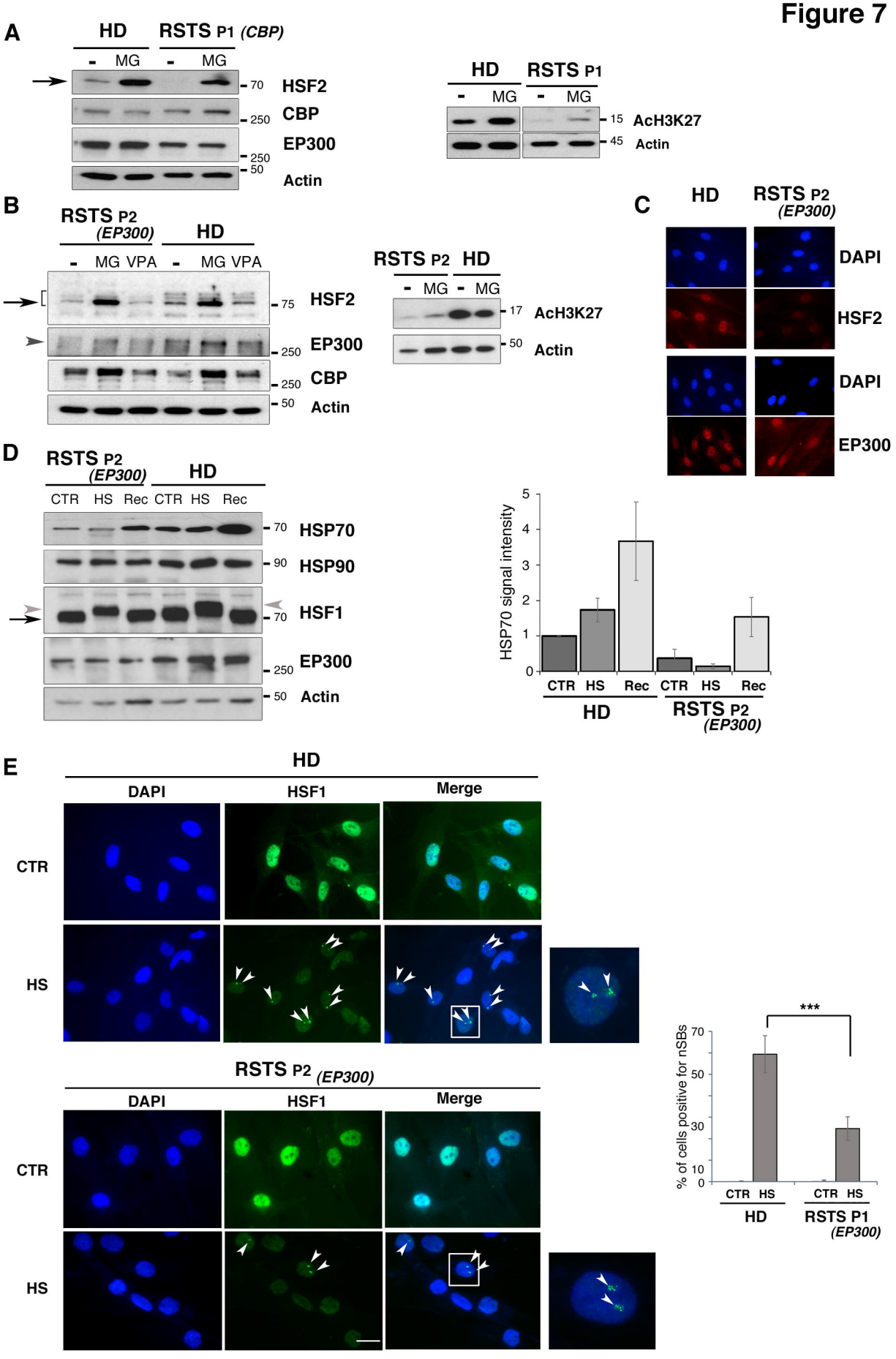
Figure 7